Monthly Notices
of the
ROYAL ASTRONOMICAL SOCIETY

Mon. Not. R. Astron. Soc. **415,** 2637–2651 (2011) doi:10.1111/j.1365-2966.2011.18889.x

Orbital evolution under the action of fast interstellar gas flow

P. Pástor,[1,2]★ J. Klačka[2]★ and L. Kómar[2]

[1]*Tekov Observatory, Sokolovská 21, 934 01 Levice, Slovak Republic*
[2]*Department of Astronomy, Physics of the Earth, and Meteorology, Faculty of Mathematics, Physics and Informatics, Comenius University, Mlynská dolina, 842 48 Bratislava, Slovak Republic*

Accepted 2011 April 8. Received 2011 April 2; in original form 2010 December 5

ABSTRACT

We investigate the orbital evolution of an interplanetary dust particle under the action of an interstellar gas flow. We present the secular time derivatives of the particle's orbital elements, for arbitrary orbit orientation. An important result concerns the secular evolution of the semimajor axis. The secular semimajor axis of the particle on a bound orbit decreases under the action of fast interstellar gas flow. In this paper, we discuss the possible types of evolution of other Keplerian orbital elements. Also, we compare the influences of the Poynting–Robertson effect, the radial solar wind and the interstellar gas flow on the dynamics of the dust particle in the outer planetary region of the Solar system and beyond, up to 100 au.

We study the evolution of a putative dust ring in the zone of the Edgeworth–Kuiper belt. The non-radial solar wind and the gravitational effect of the major planets might have an important role in this zone. We take into account both these effects. The low-inclination orbits of micrometre-sized dust particles in the belt are not stable, because of the fast increase of eccentricity caused by the long-term monodirectional interstellar gas flow and subsequent planetary perturbations – the increase of eccentricity leads to the planet-crossing orbits of the particles.

Gravitational and non-gravitational effects are treated in a way that fully respects physics. As a consequence, some of the published results have turned out to be incorrect. Moreover, in this paper we treat the problem in a more general way than it has been presented up to now.

The influence of the fast interstellar neutral gas flow should not be ignored in the modelling of the evolution of dust particles beyond planets.

Key words: celestial mechanics – interplanetary medium – ISM: general.

1 INTRODUCTION

The motion of stars relative to their local interstellar medium is a frequent/usual process in galaxies. The motion of dust particles in orbits around a star can be affected by interstellar matter penetrating into the astrosphere of the star. A star's disc of debris can show asymmetric morphology caused by the interaction of the disc with the interstellar matter. Up to now, at least three such debris discs have been detected in the neighbourhood of the Sun. The stars are HD 61005, HD 32297 and HD 15115. The morphology asymmetry of the discs, as a result of interaction of the disc with interstellar matter, has been numerically investigated by Hines et al. (2007) (HD 61005), Debes, Weinberger & Kuchner (2009) (HD 32297 and HD 15115), and others. Neutral atoms also penetrate into the Solar system as a result of the relative motion of the Sun with respect to the interstellar medium. This flow of neutral atoms through the heliosphere has been investigated in many papers (e.g. Fahr 1996; Lee et al. 2009; Möbius et al. 2009). However, the influence of the interstellar gas flow on the dynamics of dust particles in the Solar system is usually ignored in the literature. The Poynting–Robertson (PR) effect, the radial solar wind and the gravitational perturbation of a planet (planets) are usually taken into account (Šidlichovský & Nesvorný 1994; Liou & Zook 1997, 1999; Kuchner & Holman 2003).

The motion of a spherical dust particle in the Solar system under the action of the interstellar gas flow has been analytically and numerically investigated by Scherer (2000). Scherer has calculated the secular time derivatives of the particle's angular momentum and the Laplace–Runge–Lenz vector caused by the interstellar gas flow. However, Scherer's calculations contain several errors. He has come to the conclusion that the semimajor axis of the dust particle increases exponentially (Scherer 2000, p. 334). In this paper, within the framework of perturbation theory, we show that the semimajor axis of the dust particle decreases under the action of the interstellar gas flow.

★E-mail: pavol.pastor@hvezdarenlevice.sk (PP); klacka@fmph.uniba.sk (JK)

The influence of the interstellar flow of gas on the motion of dust particles in the zone of the Edgeworth–Kuiper belt has been investigated by Klačka et al. (2009a). They have calculated the secular time derivatives of orbital elements only for the case when the interstellar gas velocity vector lies in the orbital plane of the dust particle and the direction of the velocity vector is parallel with the y-axis. In this paper, we overcome these restrictions.

Belyaev & Rafikov (2010) investigated the motion of dust in the outer Solar system – behind the solar wind termination shock. They calculated the secular orbital evolutions of a spherical dust particle under the action of a constant monodirectional force (i.e. they solved the classical Stark problem; a generalized and improved solution of the classical Stark problem can be found in Pástor 2010). At usage of the classical Stark problem it is assumed that the orbital speed of the dust grain can be neglected in comparison with the speed of the interstellar gas flow. Therefore, the solution of the classical Stark problem does not describe the motion of the dust grain in the correct way. This is especially true in the vicinity of the Sun, where the orbital speed of the dust grain is high. The solution of the classical Stark problem might serve as an approximation in some cases. In this paper, we present the secular evolution of all orbital elements when the orbital velocity of the particle is taken into account. Belyaev & Rafikov (2010) reproduce our results (see the preprint of this paper, Pástor, Klačka & Kómar 2010) on the secular evolution of the semimajor axis of the particle's orbit. We focus on the dynamics of the dust grains inside the heliosphere and in the zone of the Edgeworth–Kuiper belt. Moreover, in our paper we present some basic properties of dust dynamics under the action of the interstellar gas.

2 SECULAR EVOLUTION

The acceleration of a spherical dust particle caused by a flow of neutral gas can be given in the form (Scherer 2000)

$$\frac{\mathrm{d}\boldsymbol{v}}{\mathrm{d}t} = -c_\mathrm{D}\gamma_\mathrm{H}|\boldsymbol{v}-\boldsymbol{v}_\mathrm{H}|\,(\boldsymbol{v}-\boldsymbol{v}_\mathrm{H})\,. \tag{1}$$

Here, $\boldsymbol{v}_\mathrm{H}$ is the velocity of the neutral hydrogen atom in the stationary frame associated with the Sun, $\boldsymbol{v}$ is the velocity of the dust grain, c_D is the drag coefficient and γ_H is the collision parameter. For the collision parameter, we can write

$$\gamma_\mathrm{H} = n_\mathrm{H}\frac{m_\mathrm{H}}{m}A, \tag{2}$$

where m_H is the mass of the neutral hydrogen atom, n_H is the concentration of the interstellar neutral hydrogen atoms and $A = \pi R^2$ is the geometrical cross-section of the spherical dust grain of radius R and mass m. The concentration of interstellar hydrogen n_H is not constant in the entire heliosphere. For heliocentric distances r less than 4 au, n_H decreases precipitously from its value in the outer heliosphere toward the Sun, because of ionization (Lee et al. 2009). However, in the outer heliosphere, $r \in$ (30 au, 80 au), we can assume that the concentration of the neutral hydrogen atoms is constant $n_\mathrm{H} = 0.05\,\mathrm{cm}^{-3}$ (Fahr 1996). The same assumption can also be used behind the solar wind termination shock. The shock was crossed by *Voyager 1* at the heliocentric distance 94 au and by *Voyager 2* at 84 au (Richardson et al. 2008).

We assume that the speed of interstellar gas is much greater than the speed of the dust grain in the stationary frame associated with the Sun ($|\boldsymbol{v}| = v \ll |\boldsymbol{v}_\mathrm{H}| = v_\mathrm{H}$). This approximation leads to an approximately constant value of $c_\mathrm{D} \approx 2.6$ (Baines, Williams & Asebiomo 1965; Banaszkiewicz, Fahr & Scherer 1994; Scherer 2000; Klačka et al. 2009a).

We want to find the influence of the interstellar gas flow on the secular evolution of the particle's orbit. We assume that the dust particle is under the action of the gravitation of the Sun and the flow of neutral gas. Hence, we have the equation of motion

$$\frac{\mathrm{d}\boldsymbol{v}}{\mathrm{d}t} = -\frac{\mu}{r^3}\boldsymbol{r} - c_\mathrm{D}\gamma_\mathrm{H}|\boldsymbol{v}-\boldsymbol{v}_\mathrm{H}|\,(\boldsymbol{v}-\boldsymbol{v}_\mathrm{H})\,, \tag{3}$$

where $\mu = G\,\mathrm{M}_\odot$, G is the gravitational constant, $\mathrm{M}_\odot$ is the mass of the Sun, $\boldsymbol{r}$ is the position vector of the dust particle with respect to the Sun and $r = |\boldsymbol{r}|$. From the derivation presented in Appendix A, for the secular time derivatives of the Keplerian orbital elements caused by the interstellar gas flow, we finally obtain:

$$\left\langle\frac{\mathrm{d}a}{\mathrm{d}t}\right\rangle = -2ac_\mathrm{D}\gamma_\mathrm{H}v_\mathrm{H}^2\sqrt{\frac{p}{\mu}}\sigma \times\left\{1+\frac{1}{v_\mathrm{H}^2}\left[I^2-(I^2-S^2)\frac{1-\sqrt{1-e^2}}{e^2}\right]\right\}, \tag{4}$$

$$\left\langle\frac{\mathrm{d}e}{\mathrm{d}t}\right\rangle = c_\mathrm{D}\gamma_\mathrm{H}v_\mathrm{H}\sqrt{\frac{p}{\mu}}\left[\frac{3I}{2}+\frac{\sigma(I^2-S^2)(1-e^2)}{v_\mathrm{H}e^3} \times\left(1-\frac{e^2}{2}-\sqrt{1-e^2}\right)\right], \tag{5}$$

$$\left\langle\frac{\mathrm{d}\omega}{\mathrm{d}t}\right\rangle = \frac{c_\mathrm{D}\gamma_\mathrm{H}v_\mathrm{H}}{2}\sqrt{\frac{p}{\mu}}\left\{-\frac{3S}{e}+\frac{\sigma SI}{v_\mathrm{H}e^4} \times\left[e^4-6e^2+4-4(1-e^2)^{3/2}\right]+C\frac{\cos i}{\sin i} \times\left[\frac{3e\sin\omega}{1-e^2}-\frac{\sigma}{v_\mathrm{H}}(S\cos\omega-I\sin\omega)\right]\right\}, \tag{6}$$

$$\left\langle\frac{\mathrm{d}\Omega}{\mathrm{d}t}\right\rangle = \frac{c_\mathrm{D}\gamma_\mathrm{H}v_\mathrm{H}C}{2\sin i}\sqrt{\frac{p}{\mu}} \times\left[-\frac{3e\sin\omega}{1-e^2}+\frac{\sigma}{v_\mathrm{H}}(S\cos\omega-I\sin\omega)\right], \tag{7}$$

$$\left\langle\frac{\mathrm{d}i}{\mathrm{d}t}\right\rangle = -\frac{c_\mathrm{D}\gamma_\mathrm{H}v_\mathrm{H}C}{2}\sqrt{\frac{p}{\mu}} \times\left[\frac{3e\cos\omega}{1-e^2}+\frac{\sigma}{v_\mathrm{H}}(S\sin\omega+I\cos\omega)\right]. \tag{8}$$

Here, $p = a\,(1-e^2)$,

$$\sigma = \frac{\sqrt{\mu/p}}{v_\mathrm{H}} \tag{9}$$

and the quantities

$$\begin{aligned} S &= (\cos\Omega\cos\omega-\sin\Omega\sin\omega\cos i)v_{\mathrm{H}X} \\ &\quad +(\sin\Omega\cos\omega+\cos\Omega\sin\omega\cos i)v_{\mathrm{H}Y} \\ &\quad +\sin\omega\sin i\,v_{\mathrm{H}Z}, \\ I &= (-\cos\Omega\sin\omega-\sin\Omega\cos\omega\cos i)v_{\mathrm{H}X} \\ &\quad +(-\sin\Omega\sin\omega+\cos\Omega\cos\omega\cos i)v_{\mathrm{H}Y} \\ &\quad +\cos\omega\sin i\,v_{\mathrm{H}Z}, \\ C &= \sin\Omega\sin i\,v_{\mathrm{H}X}-\cos\Omega\sin i\,v_{\mathrm{H}Y}+\cos i\,v_{\mathrm{H}Z}, \end{aligned} \tag{10}$$

are values of $A = \boldsymbol{v}_\mathrm{H}\cdot\boldsymbol{e}_\mathrm{R}$, $B = \boldsymbol{v}_\mathrm{H}\cdot\boldsymbol{e}_\mathrm{T}$ and $C = \boldsymbol{v}_\mathrm{H}\cdot\boldsymbol{e}_\mathrm{N}$ at the perihelion of the particle's orbit ($f = 0$), respectively. The value of

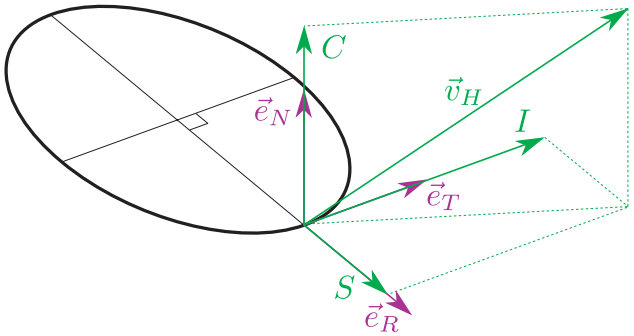

Figure 1. A schematic representation of the values S, I and C for a given orbit.

C is a constant on a given oscular orbit. The values of S, I and C are depicted in Fig. 1.

3 THEORETICAL DISCUSSION

Equations (4)–(8) enable us to deduce some properties of the secular evolution of the dust particle under the action of the flow of interstellar gas. $C = 0$ for the special case when the velocity of hydrogen gas $\boldsymbol{v}_{\rm H}$ lies in the orbital plane of the particle. In this case, we find that the inclination and the longitude of the ascending node are constant. The secular time derivatives for a special case of this type ($i = \Omega = 0$, $v_{{\rm H}X} = v_{{\rm H}Z} = 0$ and $v_{{\rm H}Y} = v_{\rm H}$ in equations 10) have been derived in Klačka et al. (2009a). The secular time derivatives of a, e and ω are given in Klačka et al. (2009a) without the generalization represented by equations (10) and Fig. 1.

Putting $\sigma = 0$ in equations (4)–(8), we obtain a solution equivalent to the solution for equation (1) with the right-hand side (rhs) independent of the particle's velocity (constant force). Equation (4) yields a constant semimajor axis for the unrealistic case $\sigma = 0$. We show, using equation (4), that the secular semimajor axis decreases under the action of interstellar gas flow for $\sigma > 0$. If the secular increase of the semimajor axis does occur, then the value of the term within the curly braces in equation (4) would be negative. The value of $1 - \sqrt{1-e^2}$ is always positive or zero. Thus, the term within the curly braces could be negative only for $I^2 - S^2 > 0$. Because S and I are the radial and transversal components of the constant vector $\boldsymbol{v}_{\rm H}$ at the perihelion (Fig. 1) of the particle orbit, we obtain the maximal value of $I^2 - S^2$ for orbit orientation characterized by $S = 0$. Using these assumptions, the minimal value (MV) within the curly braces is

$$MV = 1 + \frac{1}{v_{\rm H}^2}\left(I^2 - I^2\frac{1-\sqrt{1-e^2}}{e^2}\right)$$
$$= 1 + \frac{I^2}{v_{\rm H}^2}\sqrt{1-e^2}\frac{1-\sqrt{1-e^2}}{e^2} > 0. \qquad (11)$$

The positiveness of MV means that the secular semimajor axis is a decreasing function of time. Equation (4) was derived under the assumption that the solar gravity represents dominant acceleration in comparison to the interstellar gas disturbing acceleration. As gravitational acceleration decreases with square of a heliocentric distance, the assumption about the disturbing interstellar gas acceleration might not be valid far from the Sun. Behind the heliocentric distance at which solar gravitational acceleration equals the interstellar gas acceleration, the particle's secular semimajor axis can also be an increasing function of time. The two accelerations are equal at heliocentric distance $\approx 1 \times 10^4$ au for a dust particle with $R = 1\ \mu$m and $\varrho = 2\,{\rm g\,cm^{-3}}$ and at heliocentric distance $\approx 7 \times 10^3$ au for a dust particle with $R = 1\,\mu$m and $\varrho = 1\,{\rm g\,cm^{-3}}$. If equation (4) can be used, then the secular time derivative of the semimajor axis is proportional to the value of the semimajor axis (the value of $\sqrt{p/\mu}\sigma$ is independent of the semimajor axis).

Defining the function $w(e) \equiv 1 - e^2/2 - \sqrt{1-e^2}$, $e \in [0, 1)$, present in equation (5), we obtain

$$\frac{{\rm d}w}{{\rm d}e} \equiv \frac{\rm d}{{\rm d}e}\left(1 - \frac{e^2}{2} - \sqrt{1-e^2}\right)$$
$$= -e + \frac{e}{\sqrt{1-e^2}} \geq 0. \qquad (12)$$

Thus, $w(e)$ is an increasing function of eccentricity. We obtain that $w(e) \geq 0$ for all $e \in [0, 1)$, as $w(e)$ is an increasing function of eccentricity and $w(0) = 0$. Hence, the sign of the second term in the square brackets in equation (5) will depend only on the sign of $I^2 - S^2$.

For small values of the eccentricity, we find that the secular time derivative of eccentricity is, approximately, proportional only to the first term multiplied by I in the square brackets in equation (5).

Equation (6) yields that the argument of perihelion is constant for the planar case $C \equiv 0$ and for the orbit's orientation characterized by $S = 0$. Thus, I is also constant in this case. Therefore, the rhs of equation (5) is only a function of the orbital semimajor axis and eccentricity.

Parameters S, I and C determine the position of the orbit with respect to the interstellar gas velocity vector. Therefore, their time derivatives are useful for a description of the evolution of the orbit's position in space. Putting equations (6)–(8) into averaged time derivatives of the quantities S, I and C defined by equations (10), we obtain

$$\left\langle\frac{{\rm d}S}{{\rm d}t}\right\rangle = \frac{c_{\rm D}\gamma_{\rm H}v_{\rm H}S}{2}\sqrt{\frac{p}{\mu}}\left\{-\frac{3I}{e} - \frac{\sigma}{v_{\rm H}}\right.$$
$$\left.\times\left[C^2 - \frac{I^2}{e^4}\left(e^4 - 6e^2 + 4 - 4(1-e^2)^{3/2}\right)\right]\right\}, \qquad (13)$$

$$\left\langle\frac{{\rm d}I}{{\rm d}t}\right\rangle = \frac{c_{\rm D}\gamma_{\rm H}v_{\rm H}}{2}\sqrt{\frac{p}{\mu}}\left\{-\frac{3eC^2}{1-e^2} + \frac{3S^2}{e} - \frac{\sigma I}{v_{\rm H}}\right.$$
$$\left.\times\left[C^2 + \frac{S^2}{e^4}\left(e^4 - 6e^2 + 4 - 4(1-e^2)^{3/2}\right)\right]\right\}, \qquad (14)$$

$$\left\langle\frac{{\rm d}C}{{\rm d}t}\right\rangle = \frac{c_{\rm D}\gamma_{\rm H}v_{\rm H}C}{2}\sqrt{\frac{p}{\mu}}\left[\frac{3eI}{1-e^2} + \frac{\sigma}{v_{\rm H}}\left(S^2 + I^2\right)\right]. \qquad (15)$$

Equations (13)–(15) are not independent, because equation $S\langle{\rm d}S/{\rm d}t\rangle + I\langle{\rm d}I/{\rm d}t\rangle + C\langle{\rm d}C/{\rm d}t\rangle = 0$ always holds. Equations (13)–(15), together with equations (4) and (5), represent the system of equations that determines the evolution of the particle's orbit in space with respect to the interstellar gas velocity vector. All orbits that are created with rotations of one orbit around the line aligned with the interstellar gas velocity vector and going through the centre of gravity will undergo the same evolution determined by this system of equations.

Equations (13)–(15), together with equations (4) and (5), enable us to find some properties of the evolution of the particle's orbit in space. If σ is a small number and I is not close to zero, then we can use the following approximations of equations (5) and (13):

$$\left\langle\frac{{\rm d}e}{{\rm d}t}\right\rangle \approx \frac{3c_{\rm D}\gamma_{\rm H}v_{\rm H}}{2}\sqrt{\frac{p}{\mu}}I, \qquad (16)$$

$$\left\langle \frac{\mathrm{d}S}{\mathrm{d}t} \right\rangle \approx -\frac{3c_{\mathrm{D}}\gamma_{\mathrm{H}}v_{\mathrm{H}}}{2}\sqrt{\frac{p}{\mu}}\frac{SI}{e}. \tag{17}$$

Inserting equation (16) into equation (17) we can obtain

$$\left\langle \frac{\mathrm{d}S}{\mathrm{d}t} \right\rangle \approx -\frac{S}{e}\left\langle \frac{\mathrm{d}e}{\mathrm{d}t} \right\rangle. \tag{18}$$

This equation leads to

$$\frac{\mathrm{d}S}{S} \approx -\frac{\mathrm{d}e}{e}, \tag{19}$$

with the solution

$$S \approx \frac{U}{e}, \tag{20}$$

where U is a constant that can be determined from the initial conditions. Thus, if the major axis of the orbit is aligned with the direction of the hydrogen gas velocity vector, then the eccentricity is close to its minimal value. If σ is a small number and I and e are not close to zero, we can use the following approximation in equation (15):

$$\left\langle \frac{\mathrm{d}C}{\mathrm{d}t} \right\rangle \approx \frac{3c_{\mathrm{D}}\gamma_{\mathrm{H}}v_{\mathrm{H}}}{2}\sqrt{\frac{p}{\mu}}\frac{ICe}{1-e^2}. \tag{21}$$

If we combine equation (21) with equation (16), then we obtain

$$\left\langle \frac{\mathrm{d}C}{\mathrm{d}t} \right\rangle \approx \frac{Ce}{1-e^2}\left\langle \frac{\mathrm{d}e}{\mathrm{d}t} \right\rangle. \tag{22}$$

This equation leads to

$$\frac{\mathrm{d}C}{C} \approx \frac{e\mathrm{d}e}{1-e^2}, \tag{23}$$

with the solution

$$C \approx \frac{V}{\sqrt{1-e^2}}, \tag{24}$$

where V is an integration constant. For I, we obtain from equation $S^2 + I^2 + C^2 = v_{\mathrm{H}}^2$

$$|I| \approx \sqrt{v_{\mathrm{H}}^2 - \frac{U^2}{e^2} - \frac{V^2}{1-e^2}}. \tag{25}$$

Equations (20), (24) and (25) hold only approximately, during the evolution of the orbit in space. For a complete solution for the case $\sigma \equiv 0$, we refer the reader to Pástor (2010) and Belyaev & Rafikov (2010). It is necessary to distinguish between the Stark problem for which $\sigma \equiv 0$ and the motion of a dust particle in the gravitational field of a star for which $\sigma \neq 0$. If σ is significantly different from zero, then the terms multiplied by σ in equations (4)–(8) must be considered. In this case, the semimajor axis of the dust particle is not constant. The fact that the semimajor axis is not a constant has a direct influence on the time evolution of all orbital elements; see the semi-latus rectum $p = a(1-e^2)$ in equations (4)–(8). This conclusion is also supported by the numerical integration of the equation of motion of the dust particle (equation 3). Even if the initial conditions are identical, the time evolutions of orbital elements, for the cases $\sigma \equiv 0$ and $\sigma \neq 0$, can be significantly different. This is especially true for particles in the Edgeworth–Kuiper belt zone, because the particles in this zone have smaller semimajor axes than particles in the outer Solar system ($\sigma \sim a^{-1/2}$). Belyaev & Rafikov (2010) have investigated the dynamics of dust particles in the outer Solar system.

Now, using equations (13)–(15), we find the evolution of the particle's orbit in space for the planar case. Equation (13) yields for the planar case ($C \equiv 0$)

$$\left\langle \frac{\mathrm{d}S}{\mathrm{d}t} \right\rangle = \frac{c_{\mathrm{D}}\gamma_{\mathrm{H}}v_{\mathrm{H}}S}{2}\sqrt{\frac{p}{\mu}}\left\{ -\frac{3I}{e} + \frac{\sigma I^2}{v_{\mathrm{H}}e^4} \times \left[e^4 - 6e^2 + 4 - 4(1-e^2)^{3/2}\right] \right\}. \tag{26}$$

It is possible to show that the sign of $\langle \mathrm{d}S/\mathrm{d}t \rangle$ depends only on the signs of S and I (see Appendix B). Let us consider in the orbital plane a two-dimensional Cartesian coordinate system with the origin in the Sun and the vertical axis aligned with the direction of the hydrogen gas velocity vector. Fig. 2 depicts four such systems. The unit vector $\boldsymbol{e}_{\mathrm{RP}} = \boldsymbol{e}_{\mathrm{R}}(f = 0)$ in each of these is depicted in a different quadrant. We take into account only prograde orbits. This assumption determines the directions/orientations of the unit vectors $\boldsymbol{e}_{\mathrm{TP}} = \boldsymbol{e}_{\mathrm{T}}(f = 0)$ perpendicular to $\boldsymbol{e}_{\mathrm{RP}}$. In Fig. 2(a), $\boldsymbol{e}_{\mathrm{RP}}$ lies in the first quadrant of this coordinate system. Both scalar products $S = \boldsymbol{v}_{\mathrm{H}} \cdot \boldsymbol{e}_{\mathrm{RP}}$ and $I = \boldsymbol{v}_{\mathrm{H}} \cdot \boldsymbol{e}_{\mathrm{TP}}$ are greater than 0, for these positions of the unit vectors $\boldsymbol{e}_{\mathrm{RP}}$ and $\boldsymbol{e}_{\mathrm{TP}}$. Thus, $\langle \mathrm{d}S/\mathrm{d}t \rangle$ is negative (see Appendix B). If $\boldsymbol{e}_{\mathrm{RP}}$ lies in the second quadrant (Fig. 2b), then $\langle \mathrm{d}S/\mathrm{d}t \rangle$ is positive. If $\boldsymbol{e}_{\mathrm{RP}}$ lies in the third quadrant (Fig. 2c), then $\langle \mathrm{d}S/\mathrm{d}t \rangle$ is negative. Finally, if $\boldsymbol{e}_{\mathrm{RP}}$ lies in the fourth quadrant (Fig. 2d), then $\langle \mathrm{d}S/\mathrm{d}t \rangle$ is positive. If $\boldsymbol{e}_{\mathrm{RP}}$ is parallel with $\boldsymbol{v}_{\mathrm{H}}$, then the value of S is maximal; also, if $\boldsymbol{e}_{\mathrm{RP}}$ is antiparallel with $\boldsymbol{v}_{\mathrm{H}}$, then the value of S is minimal. Therefore, the vector $\boldsymbol{e}_{\mathrm{RP}}$ rotates counterclockwise in the first and second quadrants and clockwise in the third and fourth quadrants. Because the positions of the unit vectors $\boldsymbol{e}_{\mathrm{RP}}$ in all quadrants were chosen arbitrarily, our conclusion is general. If the vector $\boldsymbol{e}_{\mathrm{RP}}$ is parallel with the vertical axis in Fig. 2 ($I = 0$ and $C = 0$), then equation (14) yields $\langle \mathrm{d}I/\mathrm{d}t \rangle > 0$. Thus, the positions of the vector $\boldsymbol{e}_{\mathrm{RP}}$ parallel with the vertical axis in Fig. 2 are not stable. However, if $\boldsymbol{e}_{\mathrm{RP}}$ is parallel with the horizontal axis ($S = 0$ and $C = 0$), then $\langle \mathrm{d}S/\mathrm{d}t \rangle = 0$ and $\langle \mathrm{d}I/\mathrm{d}t \rangle = 0$. Thus, $\boldsymbol{e}_{\mathrm{RP}}$ parallel with the horizontal axis yields stable positions of the vector $\boldsymbol{e}_{\mathrm{RP}}$. The stable position of the vector $\boldsymbol{e}_{\mathrm{RP}}$ parallel with the horizontal axis and directed to the left in Fig. 2 is of theoretical importance only. In reality, no particles should be observed with perihelia in this direction. However, all unit vectors $\boldsymbol{e}_{\mathrm{RP}}$ of the particles in the prograde orbits will approach the right direction in Fig. 2. For retrograde orbits, we have to use the transformation $\boldsymbol{e}_{\mathrm{TP}} \rightarrow -\boldsymbol{e}_{\mathrm{TP}}$. We obtain $S \rightarrow S$, $I \rightarrow -I$ and therefore $\langle \mathrm{d}S/\mathrm{d}t \rangle \rightarrow -\langle \mathrm{d}S/\mathrm{d}t \rangle$. Hence, all unit vectors $\boldsymbol{e}_{\mathrm{RP}}$ of the particles in the retrograde orbits will approach the left direction in Fig. 2.

4 NUMERICAL RESULTS

4.1 Comparison of the numerical solution of the equation of motion and the solution of equations (4)–(8)

We have numerically solved equation (3) and the system of differential equations represented by equations (4)–(8). The solutions are compared in Fig. 3. We have assumed that the direction of the interstellar gas velocity vector is identical to the direction of the velocity of the interstellar dust particles entering the Solar system. The interstellar dust particles enter the Solar system with a speed of about $v_\infty = 26$ km s^{-1} (Landgraf et al. 1999) and they are arriving from the direction of $\lambda_{\mathrm{ecl}} = 259^\circ$ (heliocentric ecliptic longitude) and $\beta_{\mathrm{ecl}} = 8^\circ$ (heliocentric ecliptic latitude; Landgraf 2000). Thus, the components of the velocity in the ecliptic coordinates with the x-axis aligned towards the actual equinox are $\boldsymbol{v}_{\mathrm{H}} = -26$ km s^{-1} [cos(259°) cos(8°), sin(259°) cos(8°), sin(8°)]. Furthermore, we have assumed that the velocity vector and the density of

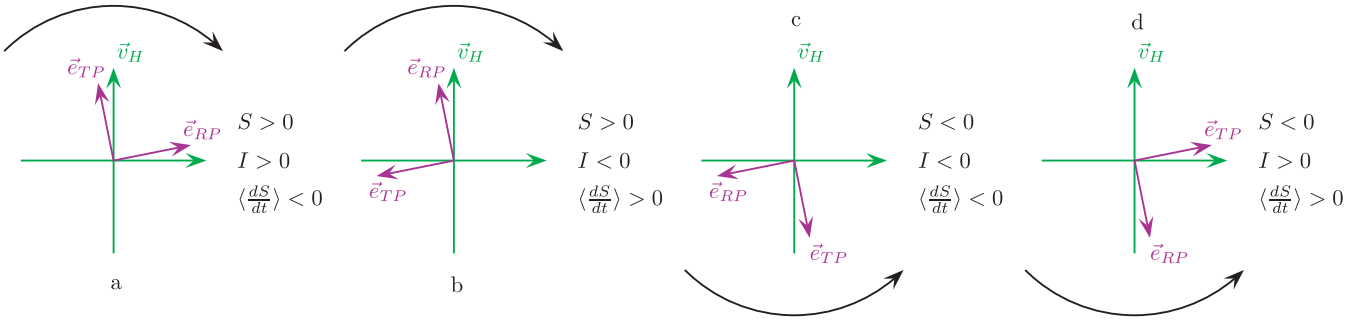

Figure 2. Secular time derivatives of S (see equations 10) for dust particles in prograde orbits in the planar case. The origins of these Cartesian coordinate systems are in the Sun and the vertical axes are aligned with the direction of the hydrogen gas velocity vector. $\boldsymbol{e}_{\rm RP}$ and $\boldsymbol{e}_{\rm TP}$ are radial and transversal unit vectors, respectively, in the perihelion of the particle orbit (see text).

the hydrogen gas atoms do not change during the time of integration of 3×10^6 yr. This assumption requires the dimension of the interstellar gas cloud to be approximately 80 pc in the direction of the hydrogen gas velocity and this cannot always be fulfilled in the real galactic environment. As the initial conditions for a dust particle with $R = 2$ μm and mass density $\varrho = 1\,\mathrm{g\,cm^{-3}}$, we used $a_{\rm in} = 60$ au, $e_{\rm in} = 0.5$, $\omega_{\rm in} = 90^\circ$, $\Omega_{\rm in} = 90^\circ$ and $i_{\rm in} = 20^\circ$ for equations (4)–(8). The initial true anomaly of the dust particle was $f_{\rm in} = 180^\circ$ for equation (3). Fig. 3 shows that the obtained evolutions are in good agreement. The evolutions begin separately as the eccentricity approaches 1. This is caused by the fact that the approximation $\sigma \ll 1$ (see equation A12) does not hold for large eccentricities. A detailed numerical solution of the equation of motion (equation 3) yields that the secular semimajor axis is also a decreasing function of time when the eccentricity approaches 1.

We can summarize, on the basis of the previous paragraph. If there is no other force, besides solar gravity and the flux of interstellar gas, then the semimajor axis of an interplanetary dust particle decreases and the particle can hit the Sun. However, the particle can also hit the Sun as a result of another possibility: the particle's eccentricity increases to 1. These mathematical possibilities probably do not occur in reality, as other forces can act on the dust particle and the interstellar gas is ionized below the heliocentric distance of about 4 au.

Let us return, once again, to the planar case ($C \equiv 0$) in which $S = 0$ and the dominant term in the square brackets in equation (5), the term $(3/2)\,I$, is negative. A numerical integration of equation (3) shows that if the eccentricity decreases to 0, then the argument of perihelion ω 'shifts' its value to the value $\omega + (2k_1 + 1)\,180^\circ$, where k_1 is an integer. This means that the negative value of I changes to positive and the eccentricity begins increase with the same slope.

The approximative solution represented by equation (20) is in good agreement with the detailed numerical solution of equations (4)–(8) for the planar case with $S \neq 0$. This holds for the whole time interval, and also for I close to zero. Equation (20) also holds, approximately, for the evolution depicted in Fig. 3. In this case, i is close to zero, $v_{\rm H} \approx v_{{\rm H}Y}$ and $\Omega \approx 90^\circ$ at the eccentricity minimum. Equation (20) gives $e \approx U/(v_{\rm H} \cos\omega)$. The evolutionary minimum of eccentricity occurs when ω is close to 180°. This is in accordance with equation (20).

We have found an interesting orbit behaviour for the case $\sigma \neq 0$. It depends on the orbit orientation with respect to the hydrogen gas velocity vector $\boldsymbol{v}_{\rm H}$. If $\boldsymbol{v}_{\rm H}$ lies in the plane $i = 0$ and $\boldsymbol{e}_{\rm RP}$ is perpendicular to $\boldsymbol{v}_{\rm H}$ (in this case $S = 0$ and $\langle {\rm d}S/{\rm d}t \rangle = 0$), then the interstellar gas flow can change a prograde orbit into a retrograde one (even more times for one particle).

4.2 Comparing the influences of interstellar gas flow, Poynting–Robertson effect and radial solar wind on the dynamics of dust particles

We have considered only the effect of interstellar gas flow, up to now. In reality, some other non-gravitational effects play non-negligible roles. Therefore, it is interesting to compare the effect of the interstellar gas flow with the other effects influencing the dynamics of dust grains in the Solar system. For this purpose, we include the PR effect and the radial solar wind in the equation of motion. The PR effect is the electromagnetic radiation pressure force acting on a spherical particle (Klačka 2004, 2008; Klačka et al. 2009c). The equation of motion of the dust particle under the action of the PR effect, the radial solar wind and the interstellar gas flow has the form (e.g. Klačka et al. 2009b)

$$\frac{{\rm d}\boldsymbol{v}}{{\rm d}t} = -\frac{\mu(1-\beta)}{r^2}\boldsymbol{e}_{\rm R} - \beta\frac{\mu}{r^2}\left(1 + \frac{\eta}{\bar{Q}'_{\rm pr}}\right)\left(\frac{\boldsymbol{v}\cdot\boldsymbol{e}_{\rm R}}{c}\boldsymbol{e}_{\rm R} + \frac{\boldsymbol{v}}{c}\right) - c_{\rm D}\gamma_{\rm H}|\boldsymbol{v} - \boldsymbol{v}_{\rm H}|\,(\boldsymbol{v} - \boldsymbol{v}_{\rm H})\,, \tag{27}$$

where the decrease of the particle's mass (corpuscular sputtering) and higher orders in $\boldsymbol{v}/c$ are neglected. c is the speed of light in vacuum. The parameter β is defined as the ratio of the electromagnetic radiation pressure force and the gravitational force between the Sun and the particle at rest with respect to the Sun:

$$\beta = \frac{3\,{\rm L}_\odot \bar{Q}'_{\rm pr}}{16\pi c G {\rm M}_\odot R \varrho},$$

$$\beta \doteq 5.763 \times 10^{-4}\frac{\bar{Q}'_{\rm pr}}{R({\rm m})\varrho({\rm kg\,m^{-3}})}. \tag{28}$$

Here, ${\rm L}_\odot$ is the solar luminosity, $L_\odot = 3.842 \times 10^{26}$ W (Bahcall 2002), $\bar{Q}'_{\rm pr}$ is the dimensionless efficiency factor for radiation pressure integrated over the solar spectrum and calculated for the radial direction ($\bar{Q}'_{\rm pr} = 1$ for a perfectly absorbing sphere) and ϱ is the mass density of the particle. η is the ratio of solar wind energy to electromagnetic solar energy, both radiated per unit of time:

$$\eta = \frac{4\pi r^2 u}{L_\odot}\sum_{i=1}^{N} n_i m_i c^2. \tag{29}$$

Here, u is the speed of the solar wind, $u = 450\,\mathrm{km\,s^{-1}}$, m_i and n_i ($i = 1$ to N) are masses and concentrations of the solar wind particles at a distance r from the Sun. $\eta = 0.38$ for the Sun (Klačka et al. 2009b). Four numerical integrations of equation (27) are shown in Fig. 4. We have used a dust particle with $R = 2$ μm, mass density $\varrho = 1$ g cm^{-3} and $\bar{Q}'_{\rm pr} = 0.75$. For the sake of simplicity, we have taken

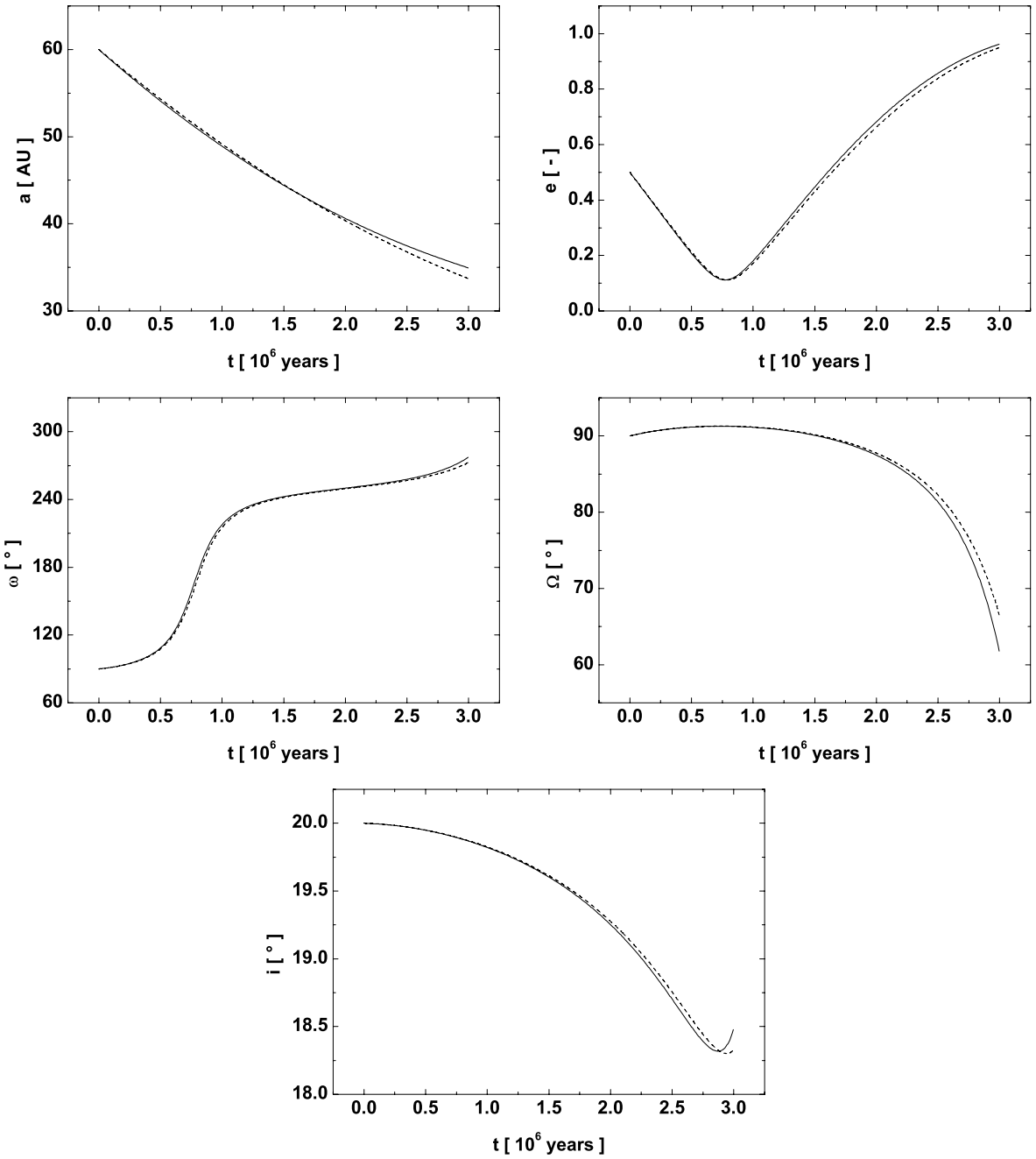

Figure 3. Two evolutions of orbital elements of a dust particle with $R = 2$ μm and mass density $\varrho = 1\,\mathrm{g\,cm^{-3}}$ under the action of interstellar gas flow. The evolution depicted by a solid line is calculated from the equation of motion. The evolution depicted by a dashed line corresponds to equations (4)–(8).

into account only the planar case when the interstellar gas velocity $\boldsymbol{v}_\mathrm{H} = (0, 26\ \mathrm{km\ s^{-1}}, 0)$ lies in the orbital plane of the dust particle ($C = 0$). The initial position is $\boldsymbol{r}_\mathrm{in} = (0, -90\ \mathrm{au}, 0)$ and the initial velocity vector is $\boldsymbol{v}_\mathrm{in} = (2\,\mathrm{km\,s^{-1}}, 0, 0)$. The orbital evolution is given by the evolution of osculating orbital elements calculated for the case when a central acceleration is defined by the first Keplerian term in equation (27), namely $-\mu(1-\beta)\boldsymbol{e}_\mathrm{R}/r^2$. This is denoted by the subscript β in Fig. 4. Mutual collisions between the dust particles are not considered (for an explanation, see Appendix C). The evolution depicted by the dash-dotted line is for the PR effect alone ($\gamma_\mathrm{H} = 0$, $\eta = 0$ in equation 27). The evolution depicted by the dotted line is for the PR effect with the flow of interstellar gas ($\eta = 0$ in equation 27). The evolution depicted by the dashed line is for the PR effect and the radial solar wind ($\gamma_\mathrm{H} = 0$ in equation 27). Finally, the evolution depicted by the solid line holds for the case when all three effects act together.

The evolution of the semimajor axis depicted in Fig. 4 shows that the flow of interstellar gas is more important than the radial solar wind, as for the effects on the dynamics of the dust particle.

The secular eccentricity is always a decreasing function of time for the PR effect and the radial solar wind (e.g. Wyatt & Whipple 1950; Klačka et al. 2009b). The growth in eccentricity depicted in Fig. 4 is a result of the interstellar gas. The fast decrease of the semimajor axis in Fig. 4 might also be, at least partially, caused by the fact that higher eccentricities decrease the value of $\langle \mathrm{d}a_\beta/\mathrm{d}t\rangle_\mathrm{PR}$ and the PR effect becomes stronger. The secular evolution of

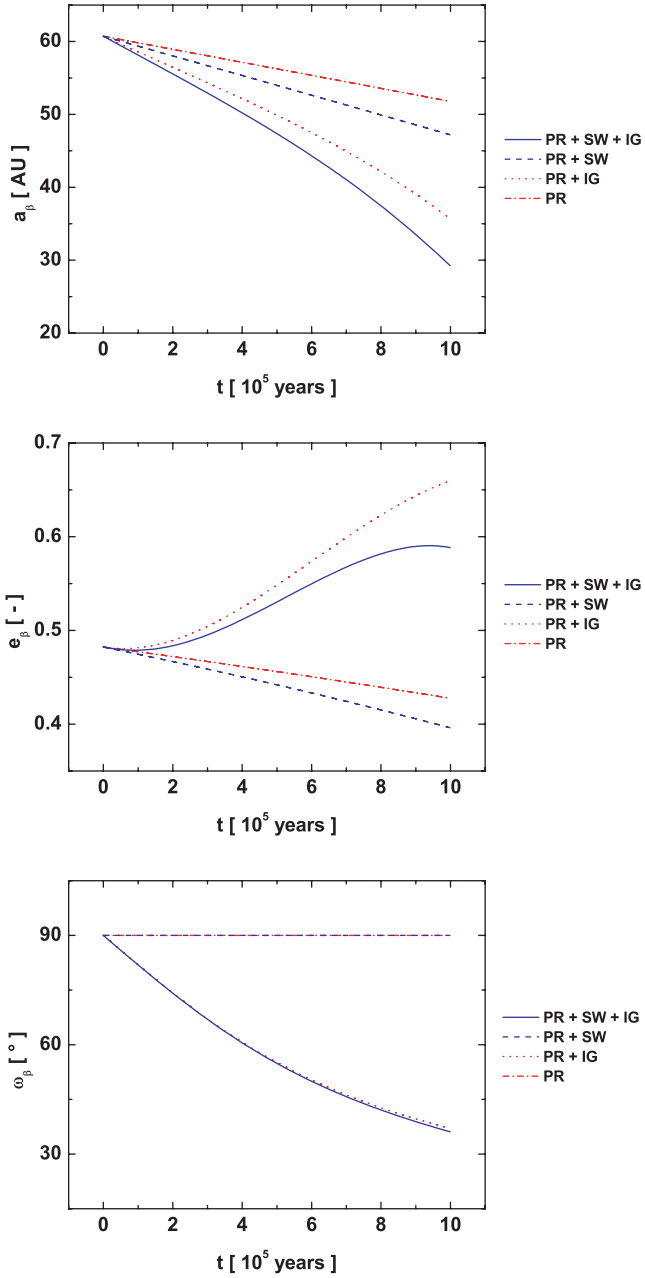

Figure 4. Orbital evolutions of a dust particle with $R = 2$ μm, mass density $\varrho = 1\,\mathrm{g\,cm^{-3}}$ and $\bar{Q}'_{\mathrm{pr}} = 0.75$ under the action of the PR effect, the radial solar wind (SW) and the flow of interstellar gas (IG).

eccentricity can be also an increasing function of time if the flow of interstellar gas is taken into account. We have

$$\left\langle \frac{\mathrm{d}e_\beta}{\mathrm{d}t} \right\rangle_{\mathrm{PR+SW+IG}} = -\frac{5}{2}\beta\left(1+\frac{\eta}{\bar{Q}'_{\mathrm{pr}}}\right)\frac{\mu}{c}\frac{e_\beta}{a_\beta^2\left(1-e_\beta^2\right)^{1/2}} + c_{\mathrm{D}}\gamma_{\mathrm{H}}v_{\mathrm{H}}\sqrt{\frac{p_\beta}{\mu(1-\beta)}} \times \left[\frac{3I_\beta}{2}+\frac{\sigma_\beta\left(I_\beta^2-S_\beta^2\right)\left(1-e_\beta^2\right)}{v_{\mathrm{H}}e_\beta^3}\left(1-\frac{e_\beta^2}{2}-\sqrt{1-e_\beta^2}\right)\right], \quad (30)$$

if equation (5) is also used. We note that the transformation $\mu \rightarrow \mu(1-\beta)$ has to be done on the rhs sides of equations (4)–(8). If we use the definition of the osculating orbital elements, then the physical central acceleration is given by the gravitational acceleration of the Sun, $-\mu \boldsymbol{e}_{\mathrm{R}}/r^2$. In this case, the secular evolution of eccentricity is given by equation (103) in Klačka (2004), assuming that e_β is calculated from equation (30).

If the optical properties of the dust particle are constant, then the secular time derivative of the argument of perihelion equals zero for the PR effect and the radial solar wind (Klačka et al. 2007; Klačka et al. 2009b). If the flow of interstellar gas is included in the equation of motion, then, even in the planar case, the secular time derivative of the argument of perihelion might not be equal to zero, in general (see Fig. 4).

The evolutions of eccentricity and the argument of perihelion shown in Fig. 4 are significantly affected by the flow of interstellar gas.

4.3 Evolution of eccentricity for various initial conditions

The complicated properties of the evolution of eccentricity shown in Fig. 4 have motivated us to explore in more detail the evolution eccentricity under the action of the solar radiation and interstellar gas flow. For this purpose, we have numerically solved equation (27) with the PR effect, radial solar wind and interstellar gas flow taken into account, similarly as in the solution for Fig. 4. For the sake of simplicity, we have solved only the planar case ($C_\beta = 0$) with the velocity of interstellar gas $\boldsymbol{v}_{\mathrm{H}} = (0,\, 26\,\mathrm{km\,s^{-1}},\, 0)$. As the initial conditions of the dust particle with $R = 2$ μm, mass density $\varrho = 1\,\mathrm{g\,cm^{-3}}$ and $\bar{Q}'_{\mathrm{pr}} = 0.75$, we used $a_{\beta\mathrm{in}} = 60$ au, $e_{\beta\mathrm{in}} \in \{0.1, 0.2, 0.3, \ldots, 0.9\}$, $\omega_{\beta\mathrm{in}} \in \{0, 45^\circ, 90^\circ, 135^\circ, 180^\circ\}$ and $f_{\beta\mathrm{in}} = 0$. Therefore, we obtained 45 individual orbits. Because of the symmetry (invariance) of the equations for secular time derivatives $\langle \mathrm{d}a/\mathrm{d}t\rangle_{\mathrm{PR+SW+IG}}$, $\langle \mathrm{d}e/\mathrm{d}t\rangle_{\mathrm{PR+SW+IG}}$, $\langle \mathrm{d}\,\omega/\mathrm{d}t\rangle_{\mathrm{PR+SW+IG}}$ after transformation $\omega_\beta \rightarrow -\omega_\beta$, it is not necessary to consider orbits with $\omega_{\beta\mathrm{in}} \in (-180^\circ, 0)$. The secular evolutions of the semimajor axis and eccentricity are identical after this transformation and the secular evolutions of the argument of perihelion are symmetric about the x-axis. Numerical integrations were stopped when the heliocentric distance of the dust particle was below 4 au. We have assumed that the concentration of interstellar hydrogen is $n_{\mathrm{H}} = 0.05\,\mathrm{cm^{-3}}$ during the whole time of integration. The results are depicted in Fig. 5.

The initial conditions used in the evolutions shown in the left panel of Fig. 5(a) ($\omega_{\beta\mathrm{in}} = 0$) yield $S_{\beta\mathrm{in}} = 0$ (see equations 10). Because ω_β has a constant zero value (equation 6), $S_\beta = 0$ also. The evolution of eccentricity shown in the left panel of Fig. 5(a) is initially an increasing function of time. This is caused by the positive value of the second term in equation (30). I_β is positive (equations 10) and the value of the second term in the square brackets in equation (30) is also positive for $S_\beta = 0$ and $I_\beta > 0$ (see also the discussion about equation 12). The interstellar gas flow is dominant on the evolution of eccentricity, for larger values of the semimajor axes, and the eccentricity is an increasing function of time. The PR effect and radial solar wind become stronger as the semimajor axis decreases, and the eccentricity begins to decrease for some critical time (see equation 30). The behaviour of the eccentricity depicted in the left panel of Fig. 5(a) is different from the behaviour expected from the solution for $\beta = 0$ and $\sigma = 0$. For the planar case, the maximum eccentricity is always 1, in the case $\beta = 0$ and $\sigma = 0$ (see Pástor 2010). This difference is caused by the inclusion of the solar radiation in the equation of motion and by the fact that σ_β is not exactly equal to zero. We can see from the evolution of eccentricity in the left panel of Fig. 5(b) ($\omega_{\beta\mathrm{in}} = 90^\circ$) that the eccentricity can only be a decreasing function of time for larger values of initial eccentricity. The increase of eccentricity

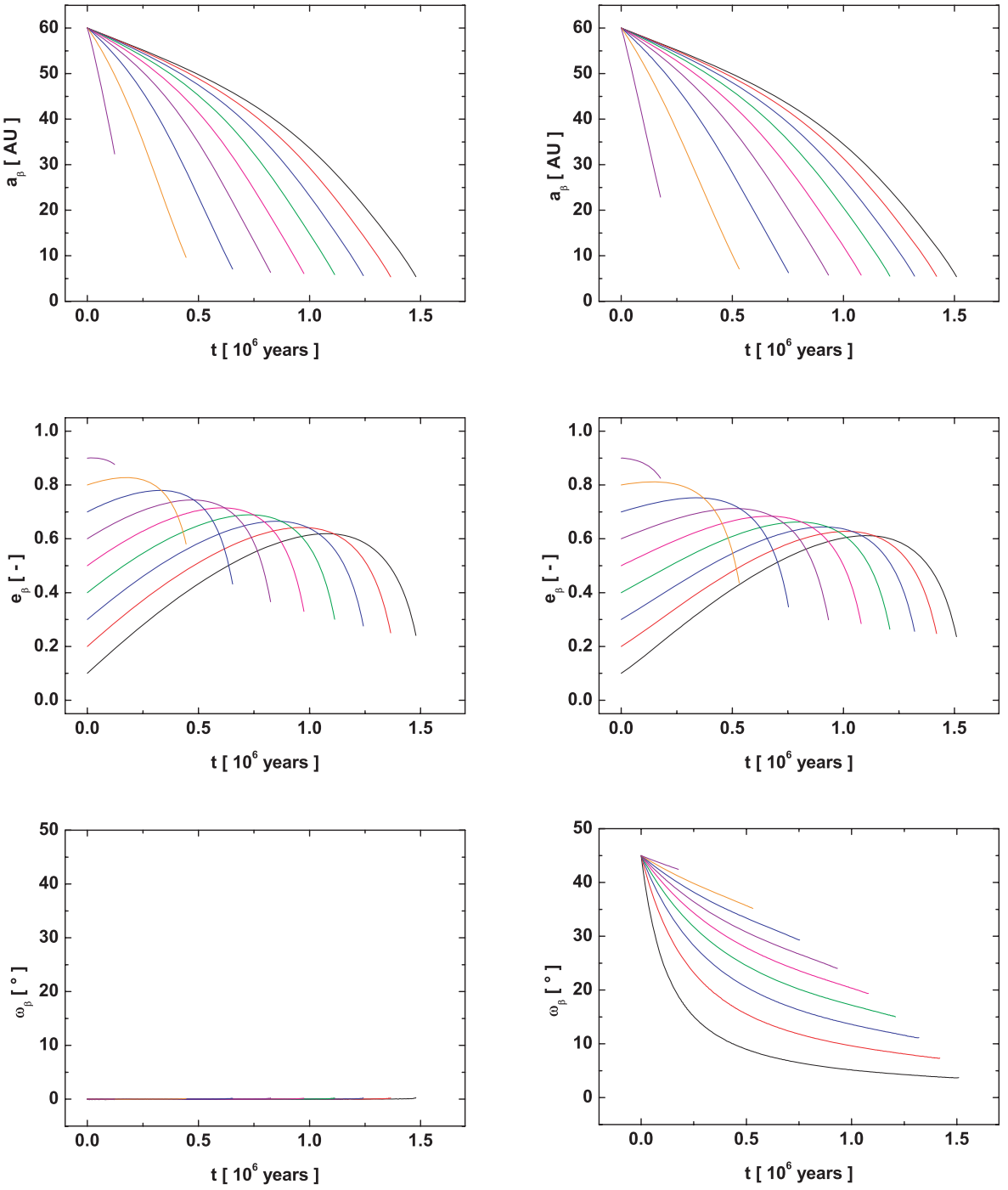

(a)

Figure 5. Orbital evolutions of a dust particle with radius $R = 2$ μm, mass density $\varrho = 1\,\mathrm{g\,cm^{-3}}$ and $\tilde{Q}'_{\mathrm{pr}} = 0.75$ under the action of the PR effect, the radial solar wind and the interstellar gas flow. (a) The initial argument of perihelion for the evolutions shown in the left panel is $\omega_{\beta\mathrm{in}} = 0$ and for evolutions shown in the right panel $\omega_{\beta\mathrm{in}} = 45^\circ$. For a given value of the argument of perihelion, we used nine various initial eccentricities. (b) The initial argument of perihelion for the evolutions shown in the left panel is $\omega_{\beta\mathrm{in}} = 90^\circ$ and for evolutions shown in the right panel $\omega_{\beta\mathrm{in}} = 135^\circ$. (c) The initial argument of perihelion for the depicted evolutions is $\omega_{\beta\mathrm{in}} = 180^\circ$.

caused by the interstellar gas flow is presented in the evolution of eccentricity only for $e_{\beta\mathrm{in}} \lesssim 0.6$ in the left panel of Fig. 5(b). The fast decrease of the eccentricity, for $e_{\beta\mathrm{in}} \gtrsim 0.6$, is because of the smaller negative value of $\langle \mathrm{d}e_\beta/\mathrm{d}t\rangle_{\mathrm{PR+SW}}$, for these values of initial eccentricities (see the first term in equation 30), and because of the zero initial value of $I_{\beta\mathrm{in}}$ (see equations 30 and 10) for this panel. However, the value of initial eccentricity, 0.6, is quite large and the majority of dust particles should undergo the increase of eccentricity caused by the interstellar gas flow. As we increase the initial value of the argument of perihelion in Fig. 5, for a given value of the initial eccentricity, the value of $I_{\beta\mathrm{in}}$ decreases (see Figs 2a and b). Therefore, the initial secular time derivative of

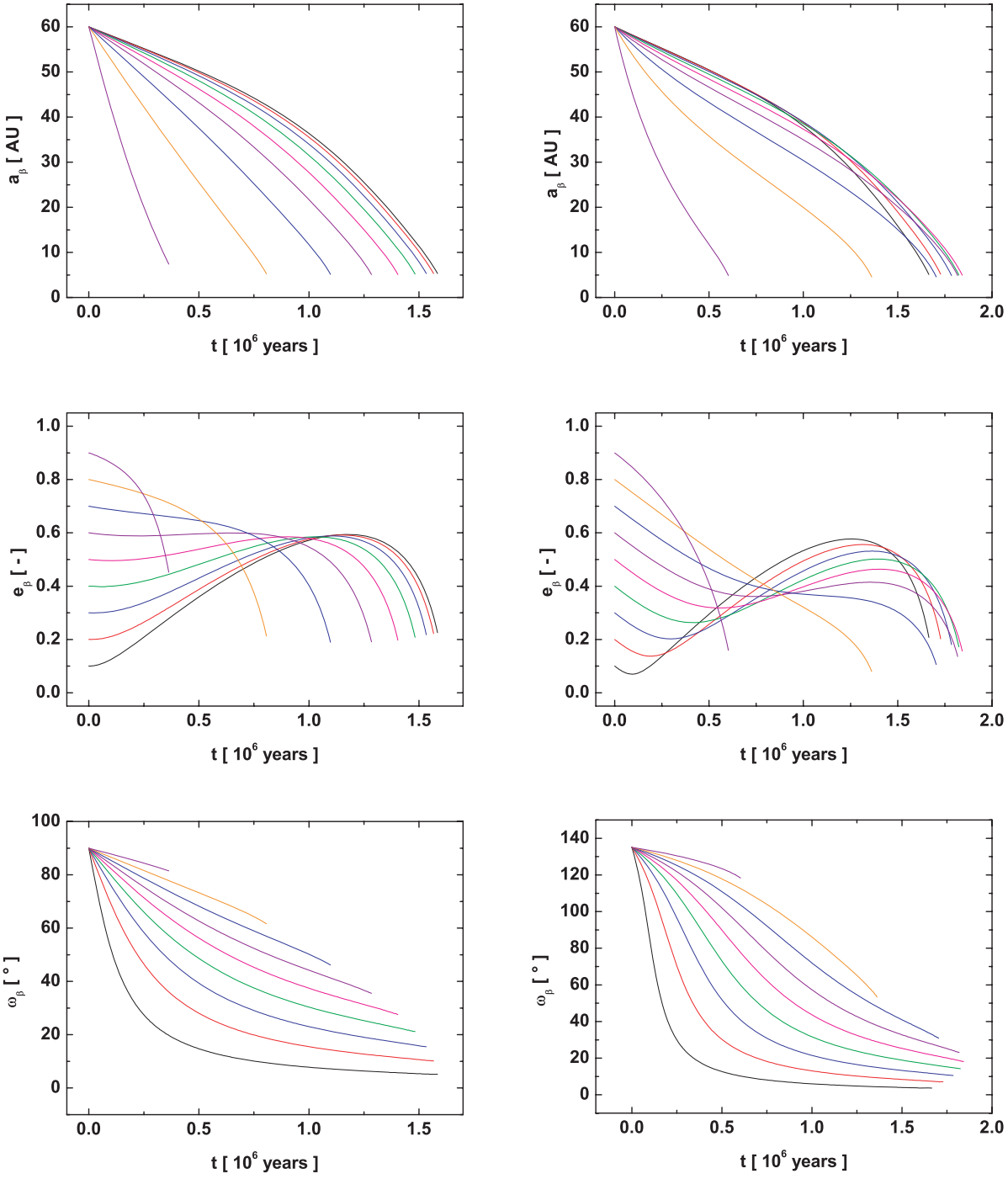

(b)

Figure 5 – *continued*

eccentricity becomes smaller. Hence, the eccentricity will initially decrease more and more precipitously for the evolutions depicted in Fig. 5.

The evolution of the semimajor axis is shortest for the particle with the greatest initial eccentricity. The fast decrease of the semimajor axis is caused by the fact that higher eccentricities decrease the value of $\langle \mathrm{d}a_\beta/\mathrm{d}t\rangle_{\mathrm{PR+SW}}$ and the influence of the PR effect and the radial solar wind becomes stronger.

The evolution of the argument of perihelion in Figs 5(a) and (b) can be described with the behaviour shown in Figs 2(a) and (b). The perihelia of orbits approach the direction with $S_\beta = 0$. For the special case $\omega_{\beta\mathrm{in}} = 180^\circ$ (see Fig. 5c), the particle's eccentricity initially decreases precipitously as a result of $I_{\beta\mathrm{in}} = -v_{\mathrm{H}}$. The eccentricity decreases to zero in some critical time. When the eccentricity reaches zero, the argument of perihelion 'shifts' its value from 180° to a value of $k_2 360^\circ$, where k_2 is an integer. This means that the eccentricity begins to increase with the same slope (as $e_\beta = 0$ is $\langle \mathrm{d}e_\beta/\mathrm{d}t\rangle_{\mathrm{PR+SW}} = 0$). The evolution of eccentricity after this moment is qualitatively equivalent with the evolutions of eccentricity depicted in the left panel of Fig. 5(a).

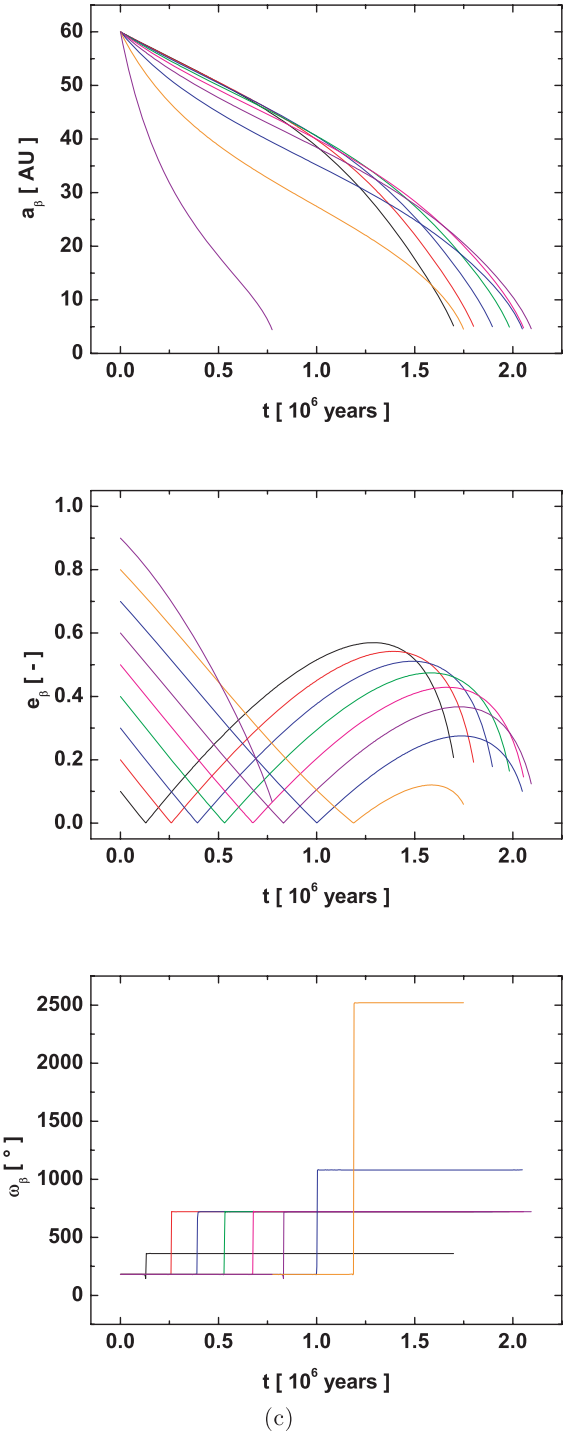

(c)

Figure 5 – *continued*

4.4 Dust ring in the Edgeworth–Kuiper belt zone

The real situation in the Edgeworth–Kuiper belt zone could be much more complicated than the situation discussed in Sections 4.1–4.3. In particular, the gravitation of planets might have an important influence on the dynamics of dust in the zone. For this reason, we have included the gravitation of four major planets in the final equation of motion. The observations from *Helios 2* during its first solar mission in 1976 (Bruno et al. 2003) show that the angle between the radial direction and the direction of the solar wind velocity does not significantly depend on heliocentric distance. If the value of this angle is approximately constant, then the non-radial solar wind can also have an important influence on the dynamics of dust in the heliosphere. We have taken into account the non-radial solar wind with the constant value of the angle. The influence of the precession of the rotational axis of the Sun on the non-radial solar wind was also considered. Hence, the equation of motion of the dust particle has the form:

$$\frac{\mathrm{d}\boldsymbol{v}}{\mathrm{d}t} = -\frac{\mu}{r^2}\boldsymbol{e}_\mathrm{R} + \beta\frac{\mu}{r^2}\left[\left(1-\frac{\boldsymbol{v}\cdot\boldsymbol{e}_\mathrm{R}}{c}\right)\boldsymbol{e}_\mathrm{R} - \frac{\boldsymbol{v}}{c}\right] - \frac{\beta\eta}{\bar{Q}'_\mathrm{pr}cu} \times \frac{\mu}{r^2}|\boldsymbol{v}-\boldsymbol{u}|\,(\boldsymbol{v}-\boldsymbol{u}) - c_\mathrm{D}\gamma_\mathrm{H}|\boldsymbol{v}-\boldsymbol{v}_\mathrm{H}|\,(\boldsymbol{v}-\boldsymbol{v}_\mathrm{H}) - \sum_{i=1}^{4}\frac{GM_i}{|\boldsymbol{r}-\boldsymbol{r}_i|^3}(\boldsymbol{r}-\boldsymbol{r}_i) - \sum_{i=1}^{4}\frac{GM_i}{|\boldsymbol{r}_i|^3}\boldsymbol{r}_i. \quad (31)$$

Here, $\boldsymbol{u}$ is the solar wind velocity vector, M_i are the masses of the planets and $\boldsymbol{r}_i$ are the position vectors of the planets with respect to the Sun. The non-radial solar wind velocity vector was calculated from the following equation

$$\boldsymbol{u} = u\left(\boldsymbol{e}_\mathrm{R}\cos\varepsilon + \frac{\boldsymbol{k}\times\boldsymbol{e}_\mathrm{R}}{|\boldsymbol{k}\times\boldsymbol{e}_\mathrm{R}|}\sin\varepsilon\right), \quad (32)$$

where ε is the angle between the radial direction and the direction of the solar wind velocity and $\boldsymbol{k}$ is a unit vector with the direction/orientation corresponding to the direction/orientation of the solar rotation angular velocity vector. The vector $\boldsymbol{k}$ for a given time can be calculated from

$$\boldsymbol{k} = (\sin\Omega_\mathrm{s}\sin i_\mathrm{s}, -\cos\Omega_\mathrm{s}\sin i_\mathrm{s}, \cos i_\mathrm{s}),$$

$$i_\mathrm{s} = 7^\circ 15',$$

$$\Omega_\mathrm{s} = 73^\circ 40' + 50.25''[t\,(\mathrm{yr}) - 1850]. \quad (33)$$

While equations (32) and (33) are consistent with Klačka (1994) and Abalakin (1986), the value of ε ($\varepsilon = 2.9^\circ$) used in our numerical calculations is in accordance with Bruno et al. (2003). The observed neutral hydrogen gas velocity vector in the ecliptic coordinates with the x-axis aligned towards the actual equinox is $\boldsymbol{v}_\mathrm{H} = -26\ \mathrm{km\,s^{-1}}$ [cos(259°) cos(8°), sin(259°) cos(8°), sin(8°)]. We have assumed that the velocity vector and the density of the hydrogen gas atoms do not change during the time of integration of 10^6 yr. This assumption requires the dimension of the interstellar gas cloud to be approximately 27 pc in the direction of the hydrogen gas velocity and this cannot be always fulfilled in the real galactic environment. As for the initial conditions of the dust particles, we have not used random positions and velocities. We have assumed that the putative dust ring in the Edgeworth–Kuiper belt has an approximate circular shape and contains many particles with approximately equal optical properties. Because the ring contains a large amount of particles, we can choose, approximately, a given value of the semimajor axis and a given radius of the particles. Accelerations caused by the PR effect, the solar wind and the interstellar neutral hydrogen gas are inversely proportional to the particle's radius and mass density. Therefore, a large particle is influenced less by the non-gravitational effects than a small particle of the same mass density. The evolution of the large particle under the action of the non-gravitational effects is typically slower than the evolution of the small dust grain. We have used uniformly distributed initial values of the argument of perihelion and the longitude of ascending node. Furthermore, we have assumed that the particles in the ring orbit prograde in low-inclination orbits. We have used particles with $R = 2$ μm,

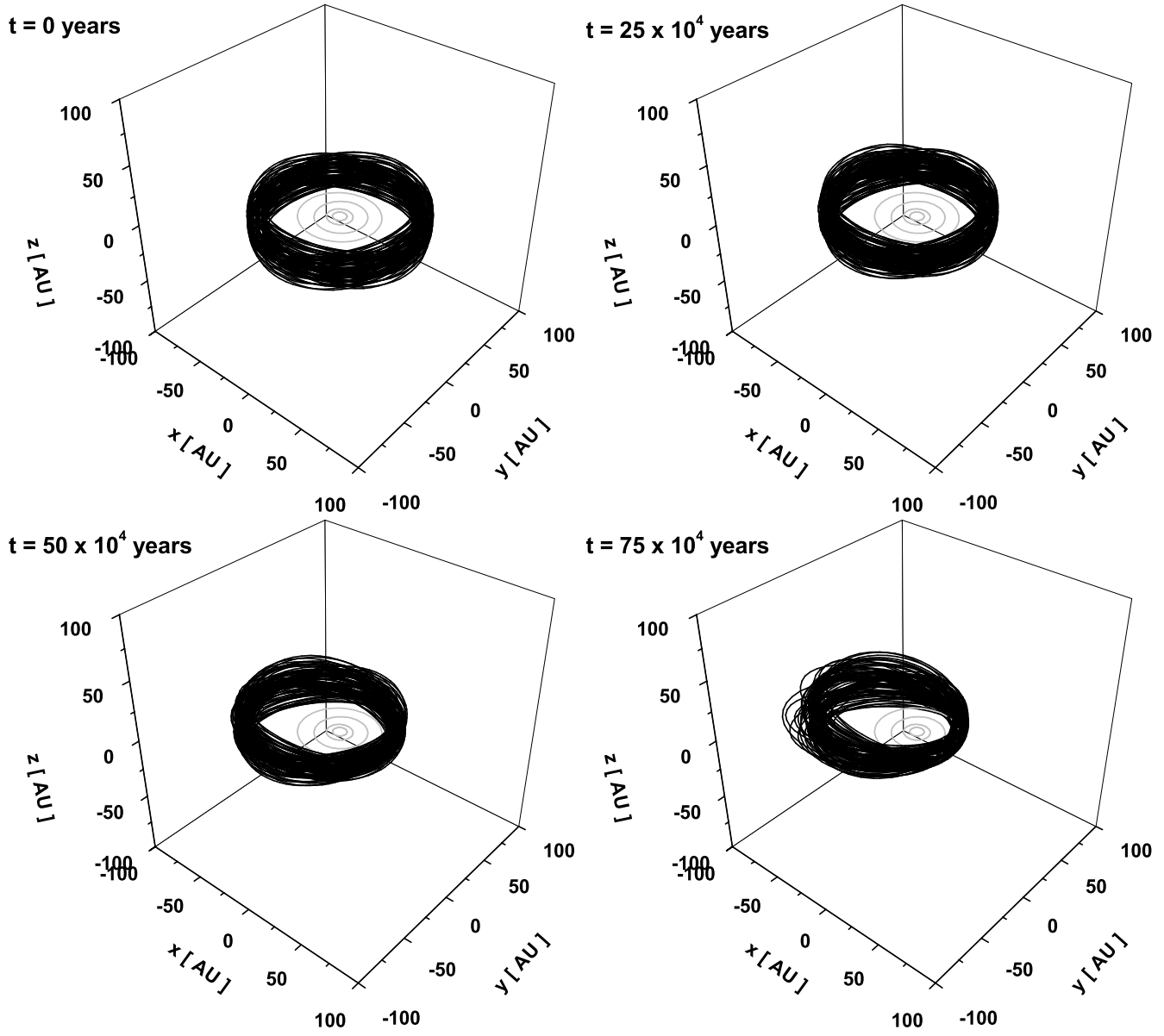

Figure 6. Time evolution of a ring of dust particles with $R = 2$ μm, $\varrho = 1\,\mathrm{g\,cm^{-3}}$ and $\bar{Q}'_{\mathrm{pr}} = 0.75$ in the zone of the Edgeworth–Kuiper belt. The ring becomes eccentric in less than 10^6 yr because of the interstellar neutral gas. The orbits of the particles are shown in black and the orbits of the planets are shown in grey.

$\varrho = 1\,\mathrm{g\,cm^{-3}}$ and $\bar{Q}'_{\mathrm{pr}} = 0.75$. The exact initial values of the orbital elements are $a_{\beta\mathrm{in}} = 60$ au, $e_{\beta\mathrm{in}} = 0.1$, $\omega_{\beta\mathrm{in}} \in \{0, 45^\circ, 90^\circ, \ldots, 270^\circ, 315^\circ\}$, $\Omega_{\beta\mathrm{in}} \in \{0, 90^\circ, 180^\circ, 270^\circ\}$, $i_{\beta\mathrm{in}} \in \{5^\circ, 10^\circ, 15^\circ\}$ and $f_{\beta\mathrm{in}} = 0$. Thus, we obtained $8 \times 4 \times 3 = 96$ individual orbits. The results of the numerical solutions of equation (31) are depicted in Figs 6 and 7. Fig. 6 depicts the evolution of the dust ring viewed in perspective. The orbits of the planets are also shown. The time-span between the various pictures in Fig. 6 is 250 000 yr. As we can see, the ring becomes more and more eccentric because of the fast increase of the eccentricity caused by the interstellar gas flow (see also the eccentricity evolution in Fig. 7). The perihelia of orbits are shifted in accordance with the behaviour, as shown in Fig. 2. This is caused by the facts that the influence of the interstellar gas flow is dominant and the solved problem is almost coplanar. The term multiplied by C^2 in equation (13) does not have a large influence on the first term in the curly braces in equation (13), in almost the coplanar case. Therefore, the lines connecting the Sun with the perihelia of particles' orbits are approaching the direction perpendicular to the interstellar gas velocity vector. The time evolution of the orbital elements of the dust particles in the ring, considered in Fig. 6, is depicted in Fig. 7. The evolutions of the argument of perihelion ω_β, beginning with a given initial value $\omega_{\beta\mathrm{in}}$, are divided into four branches because of the approach of the perihelia to one direction. Each of these corresponds to one initial value of the ascending node. If the time is less than 750 000 yr, then (i) the concentration of the particles in the ring is smallest in the direction (from the Sun) into which perihelia of the orbits are approaching and (ii) the concentration of the particles is greatest in exactly the opposite direction. If the time is greater than 750 000 yr, then the orbits of particles in the dust ring are getting close to the orbits of the planets because of the increase of particles eccentricities. The situation after 750 000 yr can be seen in Fig. 7. The locations of the exterior mean-motion resonances with a planet can be calculated from equation $a_\beta = a_{\mathrm{P}}(1 - \beta)^{1/3}\,[(j + s)/j]^{2/3}$, where j and s are

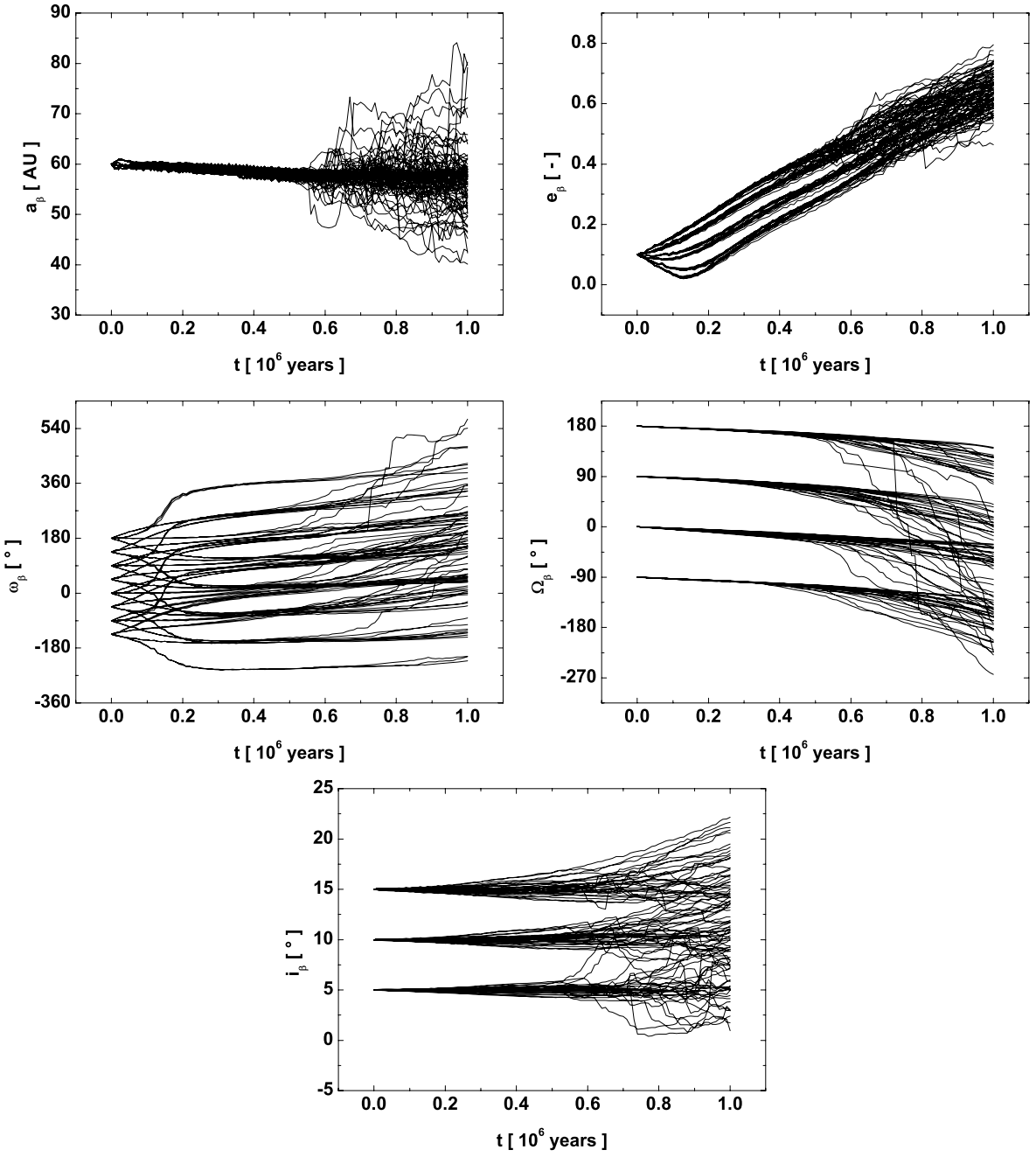

Figure 7. The evolution of orbital elements of the dust particles in the Edgeworth–Kuiper belt zone during the 96 numerical solutions depicted in Fig. 6. The initial values of the orbital elements are $a_{\beta\mathrm{in}} = 60$ au, $e_{\beta\mathrm{in}} = 0.1$, $\omega_{\beta\mathrm{in}} \in \{0, 45^\circ, 90^\circ, \ldots, 270^\circ, 315^\circ\}$, $\Omega_{\beta\mathrm{in}} \in \{0, 90^\circ, 180^\circ, 270^\circ\}$, $i_{\beta\mathrm{in}} \in \{5^\circ, 10^\circ, 15^\circ\}$ and $f_{\beta\mathrm{in}} = 0$. The evolution during the first 750 000 yr is influenced mainly by the interstellar gas and, later, mainly by the gravitation of planets (see text).

two natural numbers and a_P is the semimajor axis of the planet. The dust particles with $R = 2$ μm, $\varrho = 1\,\mathrm{g\,cm^{-3}}$ and $\bar{Q}'_\mathrm{pr} = 0.75$ are characterized by the value $\beta \approx 0.216$ (see equation 28). For this value of β, we obtain $a_\beta \approx 57.7$ au for the location of the exterior mean-motion 3/1 resonance with Neptune. We can see, from the evolution of the semimajor axis in Fig. 7, that the secular semimajor axis is a decreasing function of time during the first 750 000 yr. Thus, the semimajor axis can evolve from the initial value of 60 au to a location close to the mean-motion 3/1 resonance. Particles are influenced by both the vicinity of Neptune's orbit and the exterior mean-motion 3/1 resonance with Neptune. The evolution during the first 750 000 yr is influenced mainly by the neutral interstellar hydrogen gas and, later, mainly by the gravitation of the planets. We have compared the numerical solutions of equation (31) with and without ($i_\mathrm{s} = 0$) precession of the solar rotational axis. We have found that the precession of the solar rotational axis does not have a large influence (less than 1 per cent outside resonances) on the evolution of the dust ring.

5 CONCLUSION

We have investigated the orbital evolution of a dust grain under the action of an interstellar gas flow. We have presented the secular time

derivatives of the grain's orbital elements for an arbitrary orientation of the orbit with respect to the velocity vector of the interstellar gas. The secular time derivatives are derived using the assumptions that the acceleration caused by the interstellar gas flow is small in comparison with gravitation of a central object (the Sun), that the eccentricity of the orbit is not close to 1 and that the speed of the dust particle is small in comparison with the speed of the interstellar gas. These assumptions lead to a secular decrease of the semimajor axis a of the particle. The secular time derivative of the semimajor axis is negative and proportional to a. This result is not in accordance with that of Scherer (2000), who has stated that the semimajor axis of the particle increases exponentially. Scherer's statement is incorrect and our analytical result is confirmed by our detailed numerical integration of the equation of motion (see also Fig. 3).

If we consider only the influence of the interstellar gas flow on the orbit of the dust particle, then the product of the secular eccentricity and the magnitude of the radial component of $\boldsymbol{v}_{\mathrm{H}}$ measured in the perihelion is, approximately, constant during the orbital evolution. A simple approximative relation also holds between the secular eccentricity and the magnitude of the normal component of $\boldsymbol{v}_{\mathrm{H}}$ measured in the perihelion.

We have considered the simultaneous action of the PR effect, the radial solar wind and the interstellar gas flow. Numerical integrations have shown that the action of the flow of interstellar gas can be more important than the action of the electromagnetic and the corpuscular radiation of the Sun, as for the motion of dust particles orbiting the Sun in the outer parts of the Solar system (see Fig. 4). The physical decrease of the semimajor axis can be more than two times greater than the value produced by the PR effect and the radial solar wind. The secular evolution of eccentricity can also be an increasing function of time when we consider the PR effect and the radial solar wind together with the flow of neutral interstellar gas. This is also a relevant difference from the action of the PR effect and the radial solar wind when the secular decrease of eccentricity occurs. The simultaneous action of all three effects yields that the secular time derivative of the argument of perihelion might not be equal to zero, in general.

The gravitation of four major planets was also directly added into the equation of motion (see equation 31). This method correctly describes the capture of dust grains into mean-motion resonances with the planets. Our physical approach differs from that of Scherer (2000), who has used some type of secular access to the gravitational influence of the planets.

The assumption of the existence of a dust ring in the zone of the Edgeworth–Kuiper belt contradicts with the rapid increase of eccentricity of the ring because of an acceleration caused by long-term monodirectional interstellar gas flow. The speed of the eccentricity increase (time derivative of eccentricity) is roughly inversely proportional to the particle's size and mass density. As the eccentricity of the particles increases, the particles approach the planets. The particles in the ring are under the gravitational influence of the planets. The particles also evolve in the semimajor axis and they can be temporarily captured into mean-motion resonances. The particles can remain in chaotic orbits between the orbits of the planets or can be ejected to high eccentric orbits as a result of close encounters with one of the planets. Only particles with greater size and mass density should survive in the dust ring for a long time.

A relevant result of the paper is that the equation of motions in the form of equation (27) (or equation 31) and equations (28) and (29) have to be used in modelling of the orbital evolution of dust grains in the Solar system. The influence of the fast interstellar neutral gas flow should not be ignored in general investigations of the evolution of dust particles in the zone of the Edgeworth–Kuiper belt.

ACKNOWLEDGMENT

This paper was supported by the Scientific Grant Agency VEGA grant No. 2/0016/09.

REFERENCES

Abalakin V. K., 1986, Astronomicheskij Jezhegodnik SSSR. Nauka, Leningrad, p. 662
Bahcall J., 2002, Phys. Rev. C., 65, 025801
Baines M. J., Williams I. P., Asebiomo A. S., 1965, MNRAS, 130, 63
Banaszkiewicz M., Fahr H. J., Scherer K., 1994, Icarus, 107, 358
Belyaev M. A., Rafikov R. R., 2010, ApJ, 273, 1718
Bruno R., Carbone V., Sorriso-Valvo L., Bavassano B., 2003, J. Geophys. Res., 108 (A3), 1130
Danby J. M. A., 1988, Fundamentals of Celestial Mechanics, 2nd edn. Willmann-Bell, Richmond, VA
Debes J. H., Weinberger A. J., Kuchner M. J., 2009, ApJ, 702, 318
Fahr H. J., 1996, Space Sci. Rev., 78, 199
Fechtig H., Leinert Ch., Berg O. B., 2001, in Grün E., Gustafson B. A. S., Dermott S. F., Fechtig H., eds, Interplanetary Dust. Springer, Berlin, p. 1
Gurnett D. A., Ansher J. A., Kurth W. S., Granroth L. J., 1997, Geophys. Res. Lett., 24, 3125
Hines D. C. et al., 2007, ApJ, 671, L165
Klačka J., 1994, Earth, Moon and Planets, 64, 125
Klačka J., 2004, Celest. Mech. Dynam. Astron., 89, 1
Klačka J., 2008, preprint (arXiv:0807.2915)
Klačka J., Kocifaj M., Pástor P., Petržala J., 2007, A&A, 464, 127
Klačka J., Kómar L., Pástor P., Petržala J., 2009a, in Johannson H. E., ed., Handbook on Solar Wind: Effects, Dynamics and Interactions. NOVA Science, New York, p. 227
Klačka J., Petržala J., Pástor P., Kómar L., 2009b, preprint (arXiv:0904.2673)
Klačka J., Petržala J., Pástor P., Kómar L., 2009c, preprint (arXiv:0904.0368)
Kuchner M. J., Holman M. J., 2003, ApJ, 588, 1110
Landgraf M., 2000, J. Geophys. Res., 105, 10303
Landgraf M., Augustsson K., Grün E., Gustafson B. S., 1999, Sci, 286, 2319
Lee M. A., Fahr H. J., Kucharek H., Möbius E., Prested C., Schwadron N. A., Wu P., 2009, Space Sci. Rev., 146, 275
Liou J.-Ch., Zook H. A., 1997, Icarus, 128, 354
Liou J.-Ch., Zook H. A., 1999, AJ, 118, 580
Möbius E. et al., 2009, Sci, 326, 969
Murray C. D., Dermott S. F., 1999, Solar System Dynamics. Cambridge Univ. Press, Cambridge
Pástor P., 2009, preprint (arXiv:0907.4005)
Pástor P., 2010, preprint (arXiv:1012.1246)
Pástor P., Klačka J., Kómar L., 2010, preprint (arXiv:1008.2484)
Richardson J. D., Kasper J. C., Wang C., Belcher J. W., Lazarus A. J., 2008, Nat, 454, 63
Scherer K., 2000, J. Geophys. Res., 105, A5, 10329
Šidlichovský M., Nesvorný D., 1994, A&A, 289, 972
Wyatt S. P., Whipple F. L., 1950, ApJ, 111, 134

APPENDIX A: DERIVATION OF SECULAR TIME DERIVATIVES OF KEPLERIAN ORBITAL ELEMENTS

In equation (3), the acceleration caused by the interstellar gas flow is considered as a perturbation acceleration to the central acceleration caused by the solar gravity. In order to compute the secular time derivatives of the Keplerian orbital elements (a, the semimajor axis; e, the eccentricity; ω, the argument of perihelion; Ω, the longitude

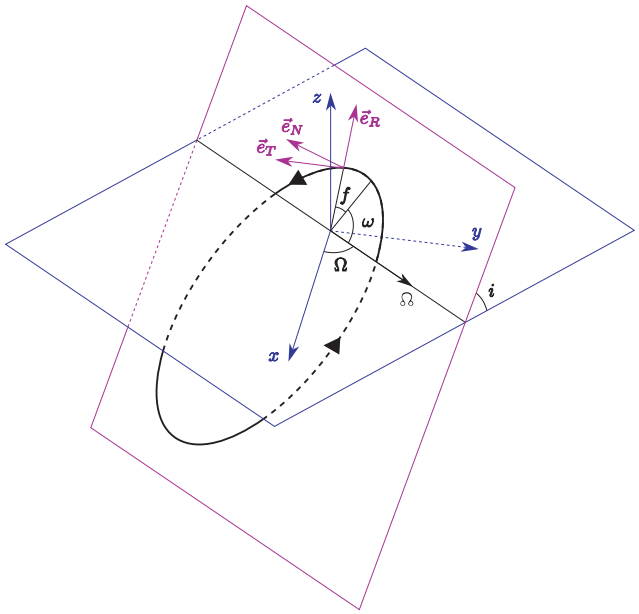

Figure A1. A particle on an elliptical orbit depicted together with the radial, transversal and normal unit vectors. The angles characterizing the position of the particle on the orbit are also shown.

of ascending node; i, the inclination), we want to use the Gaussian perturbation equations of celestial mechanics. To do this, we need to know the radial, transversal and normal components of acceleration given by equation (1). The orthogonal radial, transversal and normal unit vectors of the dust particle in the Keplerian orbit are (see Fig. A1, and, for example, Pástor 2009)

$$\begin{aligned}\boldsymbol{e}_{\mathrm{R}} = [&\cos\Omega\cos(f+\omega) - \sin\Omega\sin(f+\omega)\cos i,\\ &\sin\Omega\cos(f+\omega) + \cos\Omega\sin(f+\omega)\cos i,\\ &\sin(f+\omega)\sin i\,],\end{aligned} \tag{A1}$$

$$\begin{aligned}\boldsymbol{e}_{\mathrm{T}} = [&-\cos\Omega\sin(f+\omega) - \sin\Omega\cos(f+\omega)\cos i,\\ &-\sin\Omega\sin(f+\omega) + \cos\Omega\cos(f+\omega)\cos i,\\ &\cos(f+\omega)\sin i\,],\end{aligned} \tag{A2}$$

$$\boldsymbol{e}_{\mathrm{N}} = (\sin\Omega\sin i, -\cos\Omega\sin i, \cos i), \tag{A3}$$

where f is a true anomaly. Thus, we need to calculate the values of $a_{\mathrm{R}} = \mathrm{d}\boldsymbol{v}/\mathrm{d}t \cdot \boldsymbol{e}_{\mathrm{R}}$, $a_{\mathrm{T}} = \mathrm{d}\boldsymbol{v}/\mathrm{d}t \cdot \boldsymbol{e}_{\mathrm{T}}$ and $a_{\mathrm{N}} = \mathrm{d}\boldsymbol{v}/\mathrm{d}t \cdot \boldsymbol{e}_{\mathrm{N}}$. The velocity of the particle in an elliptical orbit can be calculated from

$$\boldsymbol{v} = \frac{\mathrm{d}\boldsymbol{r}}{\mathrm{d}t} = \frac{\mathrm{d}}{\mathrm{d}t}(r\boldsymbol{e}_{\mathrm{R}}) = r\frac{e\sin f}{1+e\cos f}\frac{\mathrm{d}f}{\mathrm{d}t}\boldsymbol{e}_{\mathrm{R}} + r\boldsymbol{e}_{\mathrm{T}}\frac{\mathrm{d}f}{\mathrm{d}t}, \tag{A4}$$

where

$$r = \frac{p}{1+e\cos f} \tag{A5}$$

and $p = a(1-e^2)$. In this calculation, the second Kepler law $\mathrm{d}f/\mathrm{d}t = \sqrt{\mu p}/r^2$ must also be used. Now, we can easily verify that

$$\begin{aligned}(\boldsymbol{v}-\boldsymbol{v}_{\mathrm{H}})\cdot\boldsymbol{e}_{\mathrm{R}} &= v_{\mathrm{H}}\sigma e\sin f - \boldsymbol{v}_{\mathrm{H}}\cdot\boldsymbol{e}_{\mathrm{R}}\\ &= v_{\mathrm{H}}\sigma e\sin f - A,\end{aligned} \tag{A6}$$

$$\begin{aligned}(\boldsymbol{v}-\boldsymbol{v}_{\mathrm{H}})\cdot\boldsymbol{e}_{\mathrm{T}} &= v_{\mathrm{H}}\sigma(1+e\cos f) - \boldsymbol{v}_{\mathrm{H}}\cdot\boldsymbol{e}_{\mathrm{T}}\\ &= v_{\mathrm{H}}\sigma(1+e\cos f) - B,\end{aligned} \tag{A7}$$

$$(\boldsymbol{v}-\boldsymbol{v}_{\mathrm{H}})\cdot\boldsymbol{e}_{\mathrm{N}} = -\boldsymbol{v}_{\mathrm{H}}\cdot\boldsymbol{e}_{\mathrm{N}} = -C, \tag{A8}$$

where

$$\sigma = \frac{\sqrt{\mu/p}}{v_{\mathrm{H}}}. \tag{A9}$$

Hence,

$$\begin{aligned}|\boldsymbol{v}-\boldsymbol{v}_{\mathrm{H}}|^2 &= v_{\mathrm{H}}^2\sigma^2(1+2e\cos f+e^2) - 2v_{\mathrm{H}}\sigma\\ &\quad\times[B+e(A\sin f + B\cos f)] + v_{\mathrm{H}}^2,\end{aligned} \tag{A10}$$

where the identity $\sqrt{A^2+B^2+C^2} = v_{\mathrm{H}}$ is used. If we denote the components of the velocity vector of hydrogen gas in the stationary Cartesian frame associated with the Sun as $\boldsymbol{v}_{\mathrm{H}} = (v_{\mathrm{H}X}, v_{\mathrm{H}Y}, v_{\mathrm{H}Z})$, then we obtain

$$\begin{aligned}A\sin f + B\cos f &= (-\cos\Omega\sin\omega - \sin\Omega\cos\omega\cos i)v_{\mathrm{H}X}\\ &+(-\sin\Omega\sin\omega + \cos\Omega\cos\omega\cos i)v_{\mathrm{H}Y}\\ &+\cos\omega\sin i\,v_{\mathrm{H}Z} = I.\end{aligned} \tag{A11}$$

Now we consider only such orbits for which

$$\sigma \ll 1, \tag{A12}$$

or, more precisely, for which the value σ^2 is negligible in comparison with σ. This is reasonable for orbits with not very large eccentricities, as $v \ll v_{\mathrm{H}}$. Using this approximation, equations (A10) and (A11) yield

$$|\boldsymbol{v}-\boldsymbol{v}_{\mathrm{H}}| = v_{\mathrm{H}}\left[1 - \frac{\sigma}{v_{\mathrm{H}}}(B+eI)\right]. \tag{A13}$$

For the radial, transversal and normal components of the acceleration, we obtain from equation (1), equations (A6)–(A8) and equation (A13):

$$a_{\mathrm{R}} = -c_{\mathrm{D}}\gamma_{\mathrm{H}}v_{\mathrm{H}}^2\left[\frac{A}{v_{\mathrm{H}}}\left(\frac{\sigma eI}{v_{\mathrm{H}}} - 1\right) + \sigma\left(e\sin f + \frac{AB}{v_{\mathrm{H}}^2}\right)\right], \tag{A14}$$

$$a_{\mathrm{T}} = -c_{\mathrm{D}}\gamma_{\mathrm{H}}v_{\mathrm{H}}^2\left[\frac{B}{v_{\mathrm{H}}}\left(\frac{\sigma eI}{v_{\mathrm{H}}} - 1\right) + \sigma\left(1 + e\cos f + \frac{B^2}{v_{\mathrm{H}}^2}\right)\right], \tag{A15}$$

$$a_{\mathrm{N}} = -c_{\mathrm{D}}\gamma_{\mathrm{H}}v_{\mathrm{H}}C\left(\frac{\sigma eI}{v_{\mathrm{H}}} - 1 + \sigma\frac{B}{v_{\mathrm{H}}}\right). \tag{A16}$$

Now we can use Gaussian perturbation equations of celestial mechanics to compute the time derivatives of the orbital elements. The perturbation equations can be found in, for example, Murray & Dermott (1999) and Danby (1988). The time average of any quantity g during one orbital period T can be computed using

$$\begin{aligned}\langle g\rangle &= \frac{1}{T}\int_0^T g\,\mathrm{d}t = \frac{\sqrt{\mu}}{2\pi a^{3/2}}\int_0^{2\pi} g\left(\frac{\mathrm{d}f}{\mathrm{d}t}\right)^{-1}\mathrm{d}f\\ &= \frac{\sqrt{\mu}}{2\pi a^{3/2}}\int_0^{2\pi} g\left(\frac{\sqrt{\mu p}}{r^2}\right)^{-1}\mathrm{d}f\\ &= \frac{1}{2\pi a^2\sqrt{1-e^2}}\int_0^{2\pi} g r^2\mathrm{d}f,\end{aligned} \tag{A17}$$

where the second ($\sqrt{\mu p} = r^2\mathrm{d}f/\mathrm{d}t$) and the third ($4\pi^2a^3 = \mu T^2$) Kepler laws are used. This procedure is used in order to derive equations (4)–(8).

APPENDIX B: SIGN OF $\langle \mathrm{d}S/\mathrm{d}t \rangle$ FOR THE PLANAR CASE

We define

$$\left\langle \frac{\mathrm{d}S}{\mathrm{d}t} \right\rangle = \frac{c_\mathrm{D}\gamma_\mathrm{H} v_\mathrm{H} S}{2}\sqrt{\frac{p}{\mu}} \times \left\{ -\frac{3I}{e} + \frac{\sigma I^2}{v_\mathrm{H} e^4}\left[e^4 - 6e^2 + 4 - 4(1-e^2)^{3/2}\right]\right\} \equiv \frac{c_\mathrm{D}\gamma_\mathrm{H} v_\mathrm{H} S}{2}\sqrt{\frac{p}{\mu}}\left[-\frac{3I}{e} + \frac{\sigma I^2}{v_\mathrm{H}} b(e)\right]. \quad \text{(B1)}$$

We need to determine if the term multiplied by σ can change the sign of the term in the square brackets in equation (B1). We have

$$b(e) = \frac{e^4 - 6e^2 + 4 - 4(1-e^2)^{3/2}}{e^4}. \quad \text{(B2)}$$

In order to find the behaviour of the function $b(e)$ we can write

$$\frac{\mathrm{d}b(e)}{\mathrm{d}e} = -\frac{4\left[4 - 4\sqrt{1-e^2} + e^2\left(-3 + \sqrt{1-e^2}\right)\right]}{e^5}, \quad \text{(B3)}$$

$$\frac{\mathrm{d}b_1(e)}{\mathrm{d}e} = \frac{\mathrm{d}}{\mathrm{d}e}\left[4 - 4\sqrt{1-e^2} + e^2\left(-3 + \sqrt{1-e^2}\right)\right] = -\frac{3e\left(-2 + e^2 + 2\sqrt{1-e^2}\right)}{\sqrt{1-e^2}}, \quad \text{(B4)}$$

$$\frac{\mathrm{d}b_2(e)}{\mathrm{d}e} = \frac{\mathrm{d}}{\mathrm{d}e}\left(-2 + e^2 + 2\sqrt{1-e^2}\right) = 2e - \frac{2e}{\sqrt{1-e^2}} \leq 0. \quad \text{(B5)}$$

Because $\mathrm{d}b_2(e)/\mathrm{d}e \leq 0$, $b_2(e)$ is a decreasing function of eccentricity. The value of $b_2(0) = 0$. Therefore, $b_2(e)$ is negative for $e \in (0, 1]$. If $b_2(e)$ is negative, then $\mathrm{d}b_1(e)/\mathrm{d}e > 0$. Therefore, $b_1(e)$ is an increasing function of eccentricity. The value of $b_1(0) = 0$. Thus, $b_1(e)$ is positive for $e \in (0, 1]$. If $b_1(e)$ is positive, then $\mathrm{d}b(e)/\mathrm{d}e < 0$. Because $\mathrm{d}b(e)/\mathrm{d}e < 0$, the function $b(e)$ is a decreasing function of eccentricity for $e \in (0, 1]$. The function $b(e)$ obtains values from $\lim_{e\to 0} b(e) = -0.5$ to $b(1) = -1$, for $e \in (0, 1]$. Because the value of the second term in the square brackets in equation (B1) is always negative, the value of the square brackets will always be negative for $I > 0$. Therefore, we assume that $I < 0$. The eccentricity $e = 1$ yields $\lim_{e\to 1} \sigma = \infty$. We deal with the values of eccentricity for which $\sigma \ll 1$ (see equation A12). Let e_m be the maximal value of the eccentricity for the case $\sigma \ll 1$. The first term in the square brackets in equation (B1) is minimal for $e = e_\mathrm{m}$ for a given negative value of I. As $b(e)$ is a decreasing function of the eccentricity and $b(e) < 0$, the negative value of the second term in the square brackets in equation (B1) will also be minimal for $e = e_\mathrm{m}$. Therefore, the use of e_m leads to the maximal influence of the term multiplied by σ on the value of the term in the square brackets in equation (B1). The second term in the square brackets yields for $e = e_\mathrm{m}$

$$\frac{\sigma I^2}{v_\mathrm{H}} b(e_\mathrm{m}) \geq -\frac{\sigma I^2}{v_\mathrm{H}} \geq \sigma I \geq I \geq 3\frac{I}{e_\mathrm{m}}, \quad \text{(B6)}$$

as $-0.5 > b(e_\mathrm{m}) > -1$, $\sigma \ll 1$ and $-I \leq v_\mathrm{H}$. If we rearrange equation (B6), then we come to the conclusion that the value of the term in the square brackets in equation (B1) will always be positive for $I < 0$ and $e \in (0, e_\mathrm{m}]$. Therefore, the term multiplied by σ in the square brackets in equation (B1) does not have any influence on the sign of the square brackets. The sign of the square brackets depends only on the sign of I. Hence, the sign of $\langle \mathrm{d}S/\mathrm{d}t \rangle$ depends only on the signs of S and I.

APPENDIX C: ESTIMATE OF MAXIMAL COLLISION RATE FOR A PARTICLE IN THE EDGEWORTH–KUIPER BELT

Voyager 1 and *Voyager 2* observed dust impacting on spacecrafts using plasma wave instruments in a range of radial heliocentric distances from 6 to 60 au. The results of Gurnett et al. (1997) show that the average number density of dust particles is about 2×10^{-8} m^{-3}, and the average mass of the particles is believed to be a few times 10^{-11} g, which corresponds to particle diameters in the micrometre range. No impacts were detected behind heliocentric distance 51 au for *Voyager 1* and 33 au for *Voyager 2* (Gurnett et al. 1997).

For the collision rate of one particle, moving between various particles with number density n, we can write

$$R_1 \approx nAv, \quad \text{(C1)}$$

where A is the collision cross-section and v is the relative velocity between impactors and target. If we neglect the PR effect, the solar wind and the interstellar gas flow, then the speed of the particle in the perihelion of a parabolic orbit at the inner edge of the Edgeworth–Kuiper belt ($r = 30$ au) is

$$v = \sqrt{\frac{2\mu}{r}} \approx 7.7\,\mathrm{km\,s^{-1}}. \quad \text{(C2)}$$

This is the maximal speed for all dust particles in the Edgeworth–Kuiper belt in bound orbits. Therefore, the maximal speed at which two particles in the Edgeworth–Kuiper belt can collide is two times higher. We use this value, 15.4 km s^{-1}, as the relative speed between the particles in estimating the maximal collision rate. Using the average number density of particles measured by the *Voyagers*, we obtain for the particle with radius $R = 2$ μm the maximal collision rate $R_1 \approx 1.2 \times 10^{-7}$ yr^{-1}. This is equivalent to one collision per eight million years, approximately.

Because the *Voyagers* were unable to detect particles with mass smaller than about 1.2×10^{-11} g (Gurnett et al. 1997), the particle number density remains unknown. If these particles were to be considered in our calculation, then the maximal collision rate could be higher. Icy particles with mass smaller than about 1×10^{-12} g are accelerated by solar radiation and follow a trajectory leaving the Solar system as the 'β-meteoroids' (Fechtig, Leinert & Berg 2001). Therefore, they do not remain in bound orbits in the Edgeworth–Kuiper belt. Because the mass of these particles was also below the detection threshold mass of the *Voyagers*, their contribution to the maximal collision rate in the Edgeworth–Kuiper belt remains unknown. A theoretical approach to the calculation of this contribution is beyond the scope of this paper.

This paper has been typeset from a TEX/LATEX file prepared by the author.